2-13-2023

Harnessing Transcriptionally driven chromosomal instability adaptation to target therapy-refractory lethal prostate cancer.

Brittiny Dhital
Mayo Clinic

Sandra Santasusagna
Mayo Clinic

Perumalraja Kirthika
Mayo Clinic

Follow this and additional works at: https://jdc.jefferson.edu/kimmelgrandrounds

Michael Xu
Thomas Jefferson University

Part of the Medical Biochemistry Commons, Medical Molecular Biology Commons, and the Oncology Commons

Peiyao Li
Thomas Jefferson University

Let us know how access to this document benefits you

See next page for additional authors

Authors

Brittiny Dhital, Sandra Santasusagna, Perumalraja Kirthika, Michael Xu, Peiyao Li, Marc Carceles-Cordon, Rajesh K. Soni, Zhuoning Li, Ronald C. Hendrickson, Matthew J. Schiewer, William K. Kelly, Cora N. Sternberg, Jun Luo, Amaia Lujambio, Carlos Cordon-Cardo, Monica Alvarez-Fernandez, Marcos Malumbres, Haojie Huang, Adam Ertel, Josep Domingo-Domenech, and Veronica Rodriguez-Bravo

Article

Harnessing transcriptionally driven chromosomal instability adaptation to target therapy-refractory lethal prostate cancer

Graphical abstract
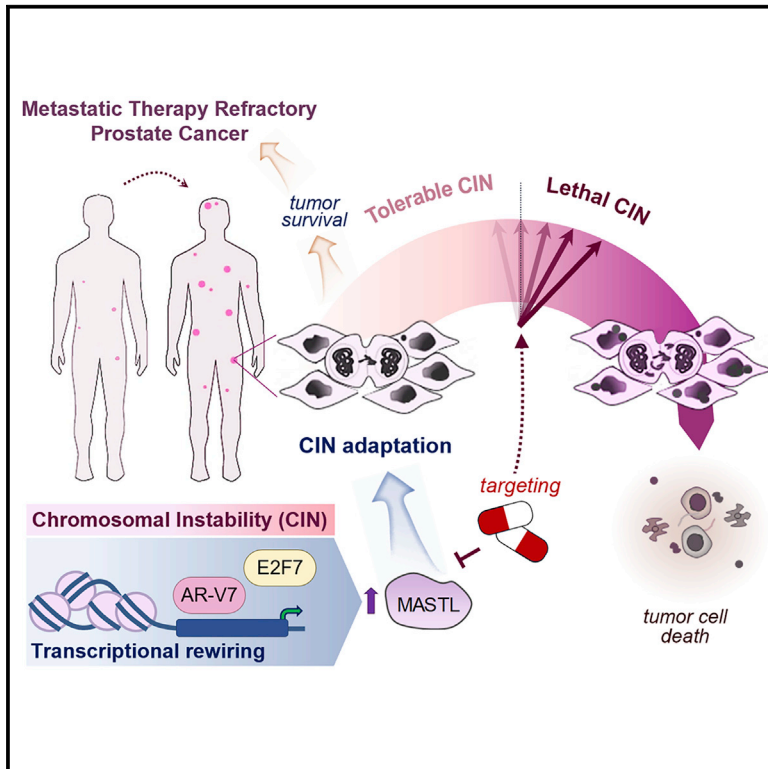
Authors

Brittiny Dhital, Sandra Santasusagna, Perumalraja Kirthika, ..., Adam Ertel, Josep Domingo-Domenech, Veronica Rodriguez-Bravo

Correspondence

domingo-domenech.josep@mayo.edu (J.D.-D.), rodriguezbravo.veronica@mayo.edu (V.R.-B.)

In brief

Dhital et al. unveil a CIN tolerance mechanism in metastatic therapy-resistant PCa involving *MASTL* upregulation by atypical transcription factors to restrain lethal chromosome defects and ensure tumor cell survival. Targeting CIN adaptation triggers tumor cell death in metastatic therapy-refractory PCa, increasing survival of pre-clinical models.

Highlights

- CIN adaptation ensures therapeutic barrier survival of lethal PCa

- MASTL kinase restrains fatal CIN levels and promotes PCa cell fitness

- AR-V7 and E2F7 transcriptional rewiring upregulate *MASTL* to promote CIN tolerance

- CIN tolerance mechanisms are a therapeutic vulnerability of lethal PCa

CelPress

Article

Harnessing transcriptionally driven chromosomal instability adaptation to target therapy-refractory lethal prostate cancer

Brittiny Dhital,[1,2,3,12] Sandra Santasusagna,[1,2,12] Perumalraja Kirthika,[1,2] Michael Xu,[3] Peiyao Li,[3] Marc Carceles-Cordon,[2] Rajesh K. Soni,[4] Zhuoning Li,[4] Ronald C. Hendrickson,[4] Matthew J. Schiewer,[3] William K. Kelly,[3] Cora N. Sternberg,[5] Jun Luo,[6] Amaia Lujambio,[7] Carlos Cordon-Cardo,[8] Monica Alvarez-Fernandez,[9] Marcos Malumbres,[10,11] Haojie Huang,[1,2] Adam Ertel,[3] Josep Domingo-Domenech,[1,2,*] and Veronica Rodriguez-Bravo[1,2,13,*]

[1]Biochemistry and Molecular Biology Department, Mayo Clinic, Rochester, MN 55905, USA
[2]Urology Department, Mayo Clinic, Rochester, MN 55905, USA
[3]Thomas Jefferson University, Sidney Kimmel Cancer Center, Philadelphia, PA 19107, USA
[4]Microchemistry and Proteomics Laboratory, Memorial Sloan Kettering Cancer Center, New York, NY 10065, USA
[5]Englander Institute for Precision Medicine, Weill Cornell Department of Medicine, Meyer Cancer Center, New York-Presbyterian Hospital, New York, NY 10021, USA
[6]Urology Department, Brady Urological Institute, Johns Hopkins University School of Medicine, Baltimore, MD 21287, USA
[7]Oncological Sciences Department, Icahn School of Medicine at Mount Sinai, New York, NY 10029, USA
[8]Pathology Department, Icahn School of Medicine at Mount Sinai, New York, NY 10029, USA
[9]Head & Neck Cancer Department, Institute de Investigación Sanitaria Principado de Asturias (ISPA), Institute Universitario de Oncología Principado de Asturias (IUOPA), 33011 Oviedo, Spain
[10]Cell Division & Cancer Group, Spanish National Cancer Research Centre (CNIO), 28029 Madrid, Spain
[11]Cancer Cell Cycle group, Vall d'Hebron Institute of Oncology (VHIO), 08035 Barcelona, Spain. Institució Catalana de Recerca i Estudis Avançats (ICREA), Barcelona, Spain
[12]These authors contributed equally
[13]Lead contact
*Correspondence: domingo-domenech.josep@mayo.edu (J.D.-D.), rodriguezbravo.veronica@mayo.edu (V.R.-B.)
https://doi.org/10.1016/j.xcrm.2023.100937

SUMMARY

Metastatic prostate cancer (PCa) inevitably acquires resistance to standard therapy preceding lethality. Here, we unveil a chromosomal instability (CIN) tolerance mechanism as a therapeutic vulnerability of therapy-refractory lethal PCa. Through genomic and transcriptomic analysis of patient datasets, we find that castration and chemotherapy-resistant tumors display the highest CIN and mitotic kinase levels. Functional genomics screening coupled with quantitative phosphoproteomics identify MASTL kinase as a survival vulnerability specific of chemotherapy-resistant PCa cells. Mechanistically, MASTL upregulation is driven by transcriptional rewiring mechanisms involving the non-canonical transcription factors androgen receptor splice variant 7 and E2F7 in a circuitry that restrains deleterious CIN and prevents cell death selectively in metastatic therapy-resistant PCa cells. Notably, MASTL pharmacological inhibition re-sensitizes tumors to standard therapy and improves survival of pre-clinical models. These results uncover a targetable mechanism promoting high CIN adaptation and survival of lethal PCa.

INTRODUCTION

Metastatic prostate cancer (PCa) remains a leading cause of death in men worldwide.[7,8] Despite effective treatments, including androgen receptor (AR) targeting and/or taxane chemotherapy,[9,10] PCa inevitably progresses to a therapy-refractory state. Therapy resistance in PCa is a consequence of cell rewiring mechanisms that can arise as adaptive responses driven by transcription factors (TFs). For example, AR amplification, gain-of-function mutations, generation of AR splice variants like AR splice variant 7 (AR-V7), or the action of master regulators TFs, among other mechanisms,

confer survival advantages to PCa cells after therapy exposure.[11,12]

Moreover, high-throughput genomic profiling is providing a more complete picture of the PCa mutational landscape during disease progression to lethal metastatic stages.[1–3,6,13–16] Different genomic dataset meta-analyses indicate that lethal PCa displays chromosomal alterations and instability like high levels of copy number alterations, fraction of genome altered (FGA), tumor mutational burden, or aneuploidy.[2,6,15–20] Indeed, chromosomal instability (CIN), the ongoing rate of chromosome segregation errors that can lead to numerical and/or structural chromosomal alterations,[21–26] is a main source of genome
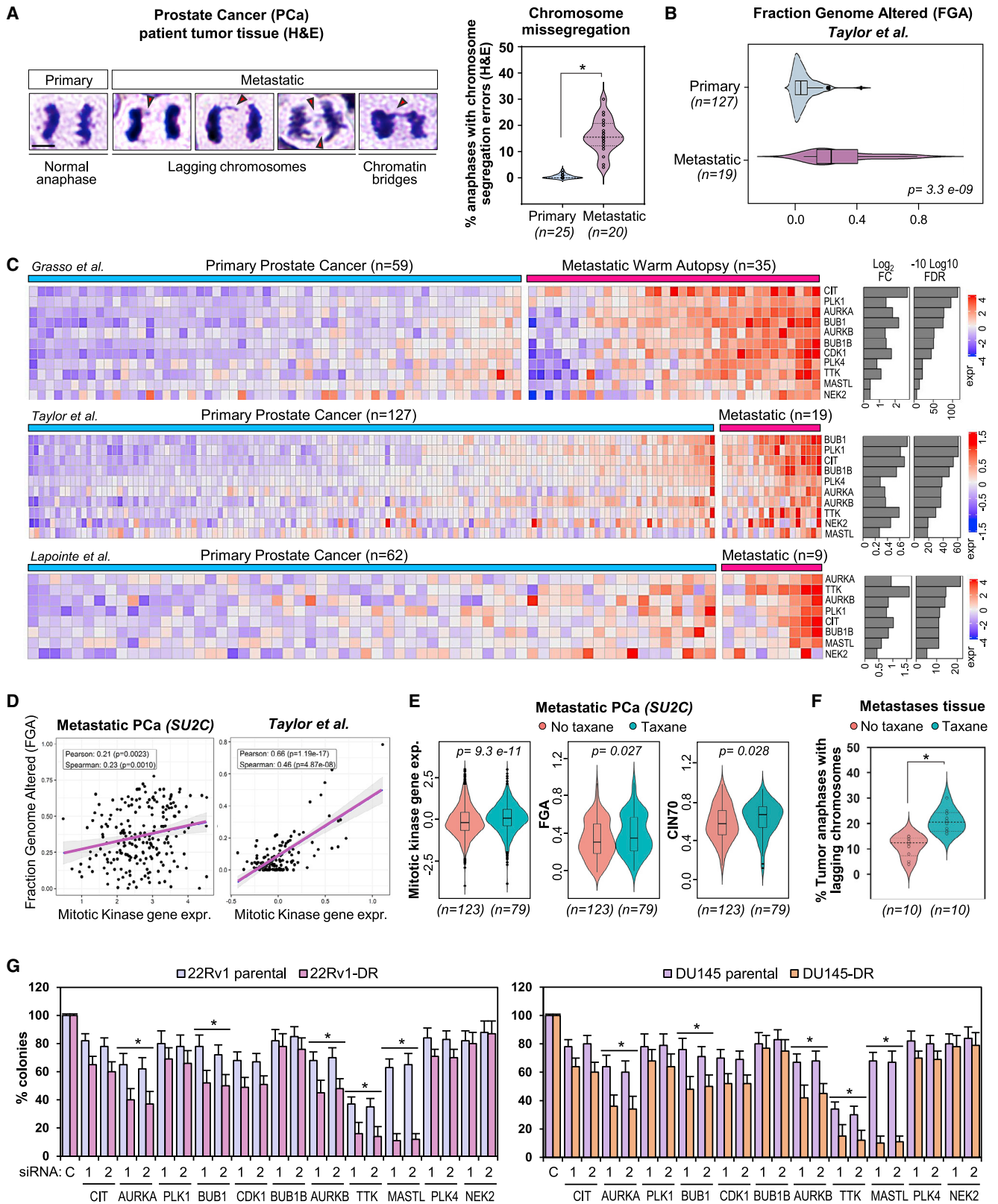
changes, tumor heterogeneity, and therapy resistance promoting tumor progression and poor clinical outcomes.[27–38] Paradoxically, severe chromosomal aberrations can also be detrimental for cancer cell growth and survival.[25,26,4,39–43] Thus, suggesting that CIN must be maintained under a tolerable threshold to preserve cancer cell homeostasis and may represent a vulnerability of aggressive tumors.[43–45] In PCa, clinical correlative studies indicate that aneuploidy and CIN associate to aggressive lethal disease[46,47]; however, the underlying causes of CIN, the adaptation mechanisms, and the potential therapeutic implications have not been studied.

Here, we investigated the molecular mechanisms promoting CIN tolerance in PCa. Interrogation of clinical patient datasets and tissues showed that CIN is highest in metastatic castration and chemotherapy-resistant PCa and is paralleled by an elevated expression of cell division fidelity kinases. Functional genomic and phosphoproteomic studies identified the upregulation of the mitotic kinase MASTL[48–51] as a key survival dependency of high CIN lethal PCa. This CIN tolerance mechanism is regulated through a transcriptional circuitry involving atypical TFs (AR-V7 and E2F7) and can be pharmacologically targeted with a MASTL small molecule inhibitor[52] that, when combined, increases the efficacy of standard therapy in patient-derived pre-clinical models. Our study uncovers CIN adaptation mechanisms that can be exploited to target therapy-refractory PCa.

RESULTS

Increased CIN and mitotic kinase gene expression confer survival vulnerabilities in metastatic therapy-refractory PCa cells

To determine the levels of CIN during PCa progression to lethal stages, we scored anaphase cells with chromosomal mis-segregation in a cohort of tissue samples containing primary and metastatic castration-resistant PCa (CRPC) tumors, as a proxy of total CIN, without distinguishing between numerical and/or structural changes (Figure 1A). We found that metastases display a higher rate of chromosome mis-segregation than primary tumors. This CIN increase was corroborated by examining the FGA, as recently described,[19] in a PCa publicly available patient dataset containing primary and metastatic tumors[2] (Figure 1B). Similar results were obtained when analyzing CIN gene signatures reported to correlate well with genome instability[4,53,5] and to predict lethality in PCa,[47] in publicly available transcriptomic PCa patient datasets[1–3] (Figure S1A and Table S1).

Chromosome mis-segregation errors originate in mitosis; therefore, we sought to determine the status of mitotic chromosomal stability maintenance pathways in lethal PCa. Interrogation of the main cell division genes in three publicly available transcriptomic patient datasets identified a subset of genes deregulated specifically in metastatic lethal PCa (Table S2), with a group of mitotic kinases distinctively upregulated in metastasis (Figure 1C). Remarkably, we identified a significant positive correlation between FGA and mitotic kinase gene expression in the Taylor dataset[2] and, most important, in the SU2C dataset,[6] which only contains metastatic PCa samples (Figure 1D). Further interrogation of treatment annotations in this dataset revealed that chemotherapy (taxane)-treated metastatic tumors displayed significantly higher mitotic kinase gene expression and FGA/CIN than non-chemotherapy-treated metastases (Figure 1E). Similar trends were observed when comparing chemo (n = 9) to non-chemotherapy-treated (n = 7) metastatic tumors from the Taylor dataset[2] (Figure S1B). Of note, significantly higher chromosome mis-segregation was also observed in a cohort of docetaxel-treated metastatic PCa tissues (Figure 1F). Thus, these analyses show increased correlation between CIN and mitotic kinase expression during PCa disease progression, being highest in metastases from taxane-treated patients.

To functionally evaluate the contribution of the clinically upregulated mitotic fidelity kinases to the viability of PCa cells, we first sought to identify suitable cell models recapitulating the high FGA/CIN and mitotic kinase gene expression observed in lethal PCa clinical samples. To this end, we scored chromosome mis-segregation by live imaging of cells expressing histone H2B-mCherry (as a measure of total CIN) and mRNA levels of mitotic kinases in a panel including normal prostate (RWPE1), primary (E006AA), metastatic hormone sensitive (LNCaP, VCaP), metastatic castration resistant (22Rv1, DU145), and syngenic chemotherapy (docetaxel)-resistant PCa cells (DR) we previously reported to recapitulate highly aggressive and multi-drug-resistant phenotypes of advanced lethal PCa.[54–57] Similar to what is observed in patient datasets, chromosome mis-segregation and mitotic kinases gene expression were increased in metastatic cells and highest in castration chemotherapy-resistant (DR) models (Figures S1C–S1E). Of note, these differences were not due to changes in cell cycle progression or proliferation between syngenic chemosensitive parental and DR cells (Figures S1F and G). We next investigated the functional relevance of the elevated CIN/mitotic kinase expression in DR cells and the potential survival dependencies by performing a focused loss-of-function genetic screen comparing the survival of syngenic parental and DR cells after knockdown of the 11 significantly increased mitotic kinases in patient datasets.[1–3] Colony formation after depletion of at least 80% of target gene mRNA with two independent small interfering

---

Figure 1. High CIN therapy-resistant PCa develops dependencies to specific chromosomal stability maintenance kinases

(A) Representative images and quantification of anaphases with chromosome segregation errors in primary and metastatic PCa patient tissue samples. Arrow points lagging chromosomes or chromatin bridges. Scale bar, 5 μm. H&E, hematoxylin and eosin.

(B) FGA analysis in primary and metastatic tumor samples from indicated PCa dataset.[2] p value, Wilcoxon's test.

(C) Transcriptome heatmaps of mitotic kinases in publicly available PCa datasets.[1–3] Fold change and statistical significance (false discovery rate [FDR]) of differential gene expression between primary and advanced PCa shown as bar graph for each gene. Red = high, blue = low.

(D) Correlation (Pearson/Spearman) between FGA/mitotic kinase gene expression in indicated PCa databases.[2,6]

(E) Mitotic kinase gene expression, FGA, and CIN70 score in taxane-treated and naive metastatic tumor samples in SU2C.[6] p values, Wilcoxon's test.

(F) Percentage of anaphases with lagging chromosomes in taxane-treated and naive metastatic PCa patient tissue samples.

(G) Colony formation quantification of parental/chemoresistant (DR) cells after control or two siRNAs targeting each indicated mitotic kinase. Data represent the mean ± standard deviation of at least three experiments. Unless indicated, *p ≤ 0.05, determined by Student's t test. See also Figure S1 and Tables S1 and S2.

A Quantitative Phosphoproteomics (SILAC)

B Phosphoproteomics (SILAC)

C

GO: Biological Process

D Top Mitotic Phosphopeptides (DR/parental p≤0.05)

Gene name	Protein name	Fold change
ENSA;ARPP19	*α-endosulfine;cAMP-regulated phosphoprotein 19*	3.5
TPX2	*Targeting protein for Xklp2; TPX2*	3.2
NUSAP1	*Nucleolar and spindle-associated protein 1*	3.0
BUB1B	*Mitotic checkpoint serine/threonine-protein kinase BUBR1*	2.5
PPP1R12A	*PP1 regulatory subunit 12A*	2.4
CHTF18	*Chromosome transmission fidelity protein 18*	2.3
MAP4	*Microtubule-associated protein 4*	2.3
KIF4A	*Chromosome-associated kinesin KIF4A*	2.3
CDCA3	*Cell division cycle-associated protein 3*	2.1
KIF22	*Kinesin-like protein KIF22*	2.1
CIT	*Citron Rho-interacting kinase*	2.1
TACC2	*Transforming acidic coiled-coil-containing protein 2*	2.0
PPP2R5D	*Protein phosphatase 2A 56 kDa regulatory subunit δ*	2.0
ANLN	*Actin-binding protein Anillin*	2.0
CENPF	*Centromere protein F*	2.0
SEPTIN9	*Septin 9*	1.9
KIF18B	*Kinesin-like protein KIF18B*	1.8

E

F

G
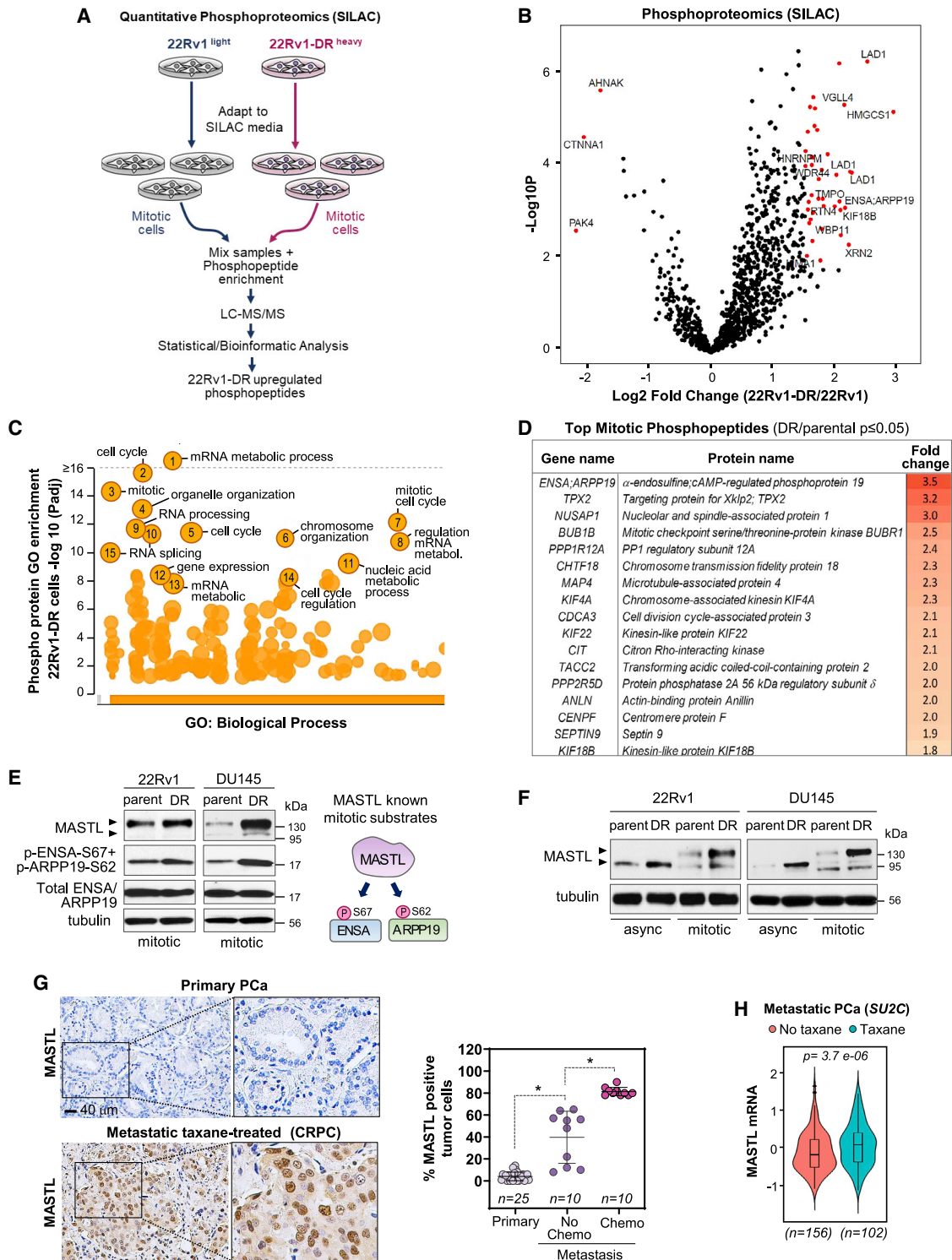

H Metastatic PCa (*SU2C*)

Figure 2. SILAC quantitative phosphoproteomic analysis identifies MASTL as a top activated mitotic kinase in therapy-resistant PCa cells

(A) Workflow of SILAC-based discovery of phosphosite changes in metastatic chemoresistant PCa cells.

(B) Volcano plot of phosphopeptide log2 fold changes comparing 22Rv1-DR and parental cells. Red dots indicate significant changes by ANOVA.

(C) Gene ontology (GO) biological process enriched in DR cells phosphoproteome (g:Profiler). p value computed by Fisher's test corrected with Benjamini-Hochberg false discovery rate.

(D) List of top upregulated cell division phosphopeptides in DR cells.

RNAs (siRNAs) (Figures S1H and S1I) identified five top chromosomal stability genes (AURKA, BUB1, AURKB, TTK, and MASTL) that, when knocked down selectively, decreased cell viability more significantly in DR than in parental cells (Figures 1G and S1J). These results suggest a concomitant increase in CIN and mitotic fidelity programs in advanced PCa, with a subset of kinases to which metastatic chemotherapy-resistant cells become selectively dependent to survive.

Quantitative phosphoproteomics identifies MASTL as a top activated chromosomal stability kinase in therapy-resistant lethal PCa

To unbiasedly identify relevant protein dependencies of high CIN metastatic therapy-resistant PCa cells, we applied a quantitative phosphoproteomic approach to compare phosphorylation changes during cell division between DR and syngenic parental cells. 22Rv1-DR and parental cells were differentially labeled to perform stable isotope labeling by amino acids in culture (SILAC) analysis[58] and arrested in mitosis to identify relevant phosphoproteomic changes when cells are close to chromosome segregation (Figure 2A). Samples were subjected to phosphopeptide enrichment and mass spectrometry followed by bioinformatic analysis to determine statistically significant differences between cells. Phosphopeptide fold changes were determined between DR and parental cells (Figure 2B and Table S3) and main biological categories enriched in the DR cells phosphoproteome identified through g:Profiler analysis,[59] including cell division/mitosis and RNA processing and stability (Figure 2C). We focused on changes in the chromosomal segregation fidelity group because of its causal connection to chromosome mis-segregation and CIN. Notably, α-endosulfine (ENSA) and ARPP19 (cyclic AMP-regulated phosphoprotein 19) were the top hyper-phosphorylated proteins in DR cells compared with parental cells (Figure 2D and Table S4). Since these are the only two known substrates of MASTL, a kinase controlling mitotic entry, progression, and genome stability,[48,49,51] this approach unequivocally identified increased MASTL activity specifically in therapy-resistant metastatic PCa cells. The increase in phosphorylated ENSA and ARPP19 in 22Rv1-DR was corroborated in two other therapy-resistant cell models (DU145-DR and VCaP-DR) by immunoblot using a specific antibody against the phosphoresidues identified by SILAC (S67 and S62, respectively) and described in the literature as unique sites of phosphorylation by MASTL.[60,61] The higher phosphorylation was not due to an increase in total ENSA/ARPP19 protein, as indicated by immunoblot or by total proteome analysis performed in parallel (Figures 2E and S2A–S2C). These results correlated with increased MASTL protein in DR cells in both mitotic and asynchronous populations (Figures 2F and S2D) and, as shown above, are not associated with a higher accumulation of DR cells in G2/M (Figures S1F and S1G).

Last, we evaluated the clinical significance of MASTL by immunohistochemistry (IHC) analysis in a cohort of patient tumor samples, confirming the highest levels in metastatic taxane-treated tumors (Figure 2G). Similarly, a MASTL mRNA increase was observed in taxane-treated metastatic samples from PCa patients (SU2C database)[6] (Figure 2H). Overall, these data indicate a clinically relevant upregulation of MASTL kinase in therapy-refractory lethal PCa, providing a rationale to mechanistically investigate its role in this disease context.

Lethal therapy-resistant PCa cells upregulate MASTL to counteract deleterious CIN

Our experimental and patient specimen results point toward a clinically significant role of MASTL upregulation in lethal therapy-refractory PCa. We further confirmed the selective MASTL survival dependency in DR cells, as indicated by increased cell death (cleaved PARP) and decreased colony formation after MASTL depletion when compared with parental cells (Figures 3A, 3B and S3A). The same results were obtained using CRISPR-Cas9 to disrupt MASTL with a previously validated sgRNA[62] (Figures 3C and 3D). Of note, the DR survival dependency was MASTL specific and dependent on its kinase activity as doxycycline inducible expression of wild-type (WT) siRNA-resistant FLAP-MASTL rescued colony formation and cell death when compared with empty vector (EV) or MASTL kinase dead (KD; G44S) (Figures 3E, 3F and S3B).

Because the main known canonical biological function of MASTL is related to cell division fidelity, we investigated whether chromosome segregation differences between DR and chemosensitive cells could explain the high sensitivity of DR cells to MASTL loss of function. To this end, we scored anaphase lagging chromosomes and kinetochores through immunofluorescence microscopy and found that MASTL depletion triggered a greater increase in chromosome mis-segregation in DR cells than in parental cells (Figure 3G), a phenotype rescued by WT MASTL kinase, but not by the catalytically inactive form (Figure S3C). Similar results were obtained in a third metastatic PCa cell model (VCaP-DR/VCaP) (Figure S3D) and by single-cell live imaging to score lagging chromosomes in MASTL-depleted histone H2B-mCherry cells (Figures S3E and S3F, and Video S1). In addition, acceleration of mitotic exit (Figure S3G) and increase in other deleterious mitotic errors like failed cytokinesis (multinucleation), centromere-positive and -negative micronuclei, or multipolar spindles were also observed in MASTL-depleted DR cells (Figures S3H and S3I). Of note, doxycycline-induced MASTL upregulation in parental cells lowered the rate of lagging chromosomes when compared with EV controls (Figures S3J and S3K).

Similar results were obtained in vivo comparing DR and parental cells stably expressing two inducible short hairpin RNAs (shRNAs) targeting MASTL (Figure S3L) subcutaneously

---

(E) MASTL, total and phospho-ENSA/ARPP19 immunoblots in mitotic cell extracts.

(F) MASTL immunoblots in asynchronous or mitotic arrested cells.

(G) MASTL IHC images and quantifications in primary, metastatic taxane-treated, and naive tumor samples from PCa patient. *p ≤ 0.05 determined by Student's t test.

(H) MASTL mRNA levels in taxane-treated and naive metastatic tumor samples in the SU2C patient dataset.[6] p value determined by Wilcoxon's test. Arrows, MASTL mobility shift changes in mitosis. See also Figure S2 and Tables S3 and S4.
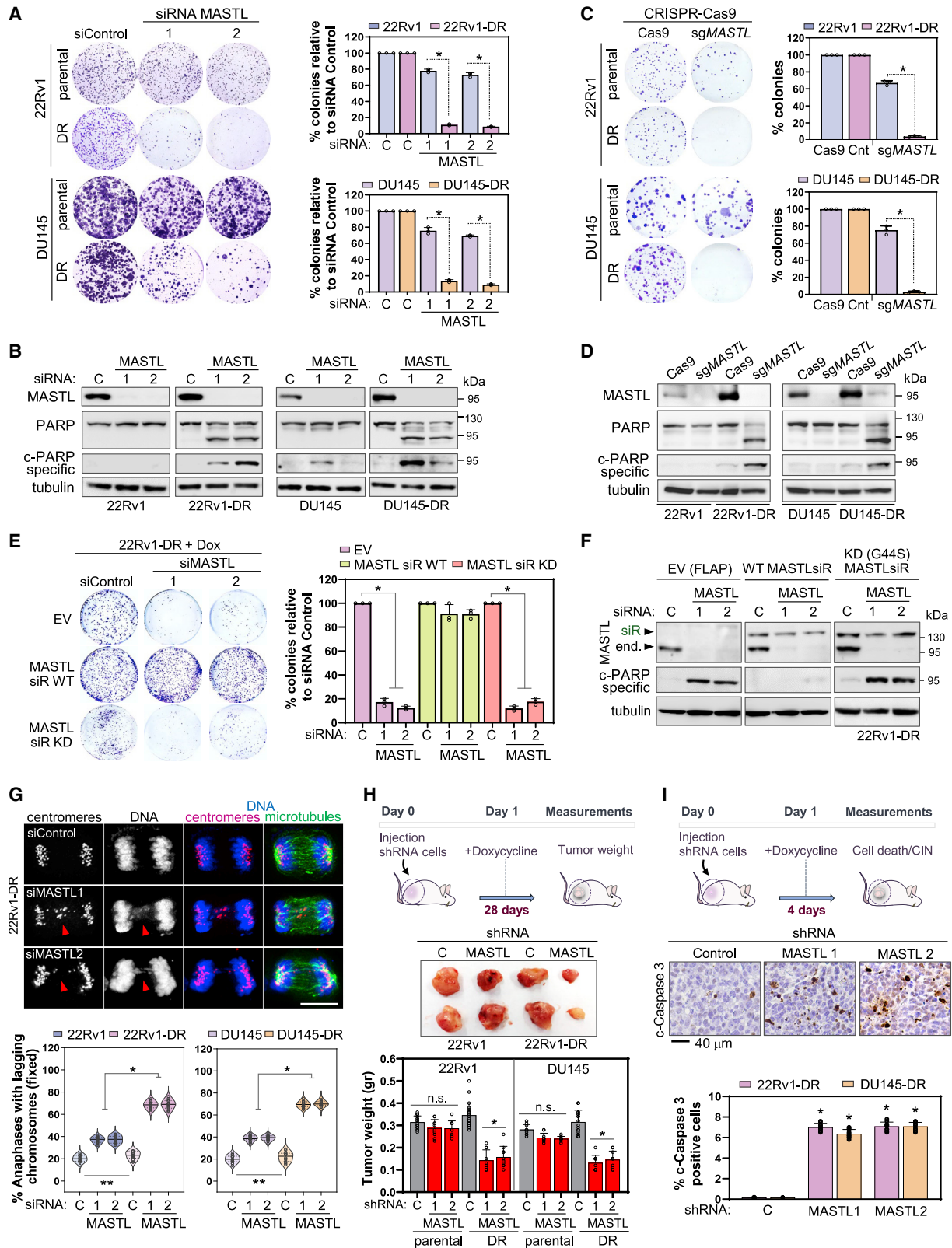
(legend on next page)

injected in the flanks of immunocompromised male mice. Doxycycline administration induced a significant decrease in tumor weight mainly in DR shRNA MASTL xenografts (Figure 3H). Notably, DR shRNA MASTL established tumors displayed increased anaphases with chromosome segregation errors (Figure S3M) and cell death (Figure 3I) than control tumors after 4 days of doxycycline exposure. Overall, these results suggest that therapy-refractory PCa displays a selective dependency on MASTL kinase activity to survive high CIN.

AR-V7 transcriptionally regulates *MASTL* expression in therapy-resistant lethal PCa cells

We next sought to investigate the upstream mechanisms promoting CIN adaptation via MASTL upregulation in lethal PCa. To this end, we performed an unbiased bioinformatic analysis to determine TFs enriched in high CIN prostate tumors from publicly available patient datasets,[2,6,63] coupled with examination of the *MASTL* promoter to identify binding sites of specific TFs[64] (Figure 4A and Table S5A). This analysis identified AR-V7 as one of the top TFs positively correlated with FGA levels and CIN in patient PCa samples (Figures 4B and S4A–S4C, and Tables S5A and S5B). AR-V7 is a constitutively active AR splice variant generated as an anti-androgen therapy resistance mechanism in metastatic CRPC patients and associated with disease progression.[65–72] Despite being clinically relevant, AR-V7's functional role in the biology of CRPC remains poorly understood.[73] Based on our results and on the paramount clinical significance of AR signaling in PCa,[74] we decided to investigate the role of AR-V7 in the transcriptional regulation of *MASTL*. Of note, analysis of two recent datasets showed decrease in MASTL mRNA after AR variants (ARVs) depletion[75,76] (Figure 4C), supporting a potential role in MASTL transcriptional regulation. Furthermore, the *MASTL* promoter contains an AR binding element that resembles previously reported ARV preferential binding sites (ARV-PBS)[75] 890 bp upstream of the transcription start site (TSS) (Figure 4D). To functionally dissect the role of AR signaling in the transcriptional control of *MASTL*, we compared the impact of both AR full length (AR-FL) and AR-V7 depletion on its gene expression in PCa cell models expressing AR-V7 and observed that, while AR-V7 knockdown significantly decreased MASTL mRNA and protein levels (Figures 4E, 4F, S4D and S4E), AR-FL depletion had no effect (Figures 4E, 4F, S4E and S4F).

These results were confirmed in AR-V7-negative PCa cells (LNCaP and C4-2) (Figures S4G–S4I).

Next, we analyzed publicly available AR-V7 chromatin immunoprecipitation (ChIP)-sequencing data and identified MASTL promoter occupancy in PCa cells[77] (Figure S4J) that we confirmed in 22Rv1-DR cells, which display the highest MASTL levels, using the same validated AR-V7 ChIP-sequencing antibody[77–79] (Figure 4G). ChIP-quantitative PCR (qPCR) analyses corroborated that AR-V7, and not AR-FL, occupies the identified ARV-PBS, but not adjacent regions, in the *MASTL* promoter (Figures 4H and S4K), and luciferase reporter assays further proved AR-V7 direct binding and activation of transcription from a WT *MASTL* promoter, while mutation of the AR-V7 binding motif significantly reduced this effect and AR-FL did not induce luciferase activity (Figure S4L). Interestingly, we observed a higher AR-V7 enrichment at *MASTL* promoter in DR cells concomitant to increased AR-V7/MASTL protein expression (Figures 4I and 4J). These results indicate that chemotherapy-resistant metastatic PCa cells increase MASTL levels through AR-V7 direct promoter binding. Notably, AR-V7 depletion recapitulated the mitotic phenotypes of MASTL perturbation and were partially rescued by MASTL overexpression, further supporting a relevant role of the AR-V7/MASTL axis in regulating chromosome segregation fidelity in metastatic therapy-resistant PCa cells (Figure S4M).

To assess a potential role of the AR-V7/MASTL axis in promoting survival to docetaxel, we transduced C4-2 cells (AR positive/AR-V7 negative) with an AR-V7 or EV and assessed effects on docetaxel sensitivity. AR-V7 expression increased C4-2 cells MASTL levels and activity (Figure 4K, left and middle) and survival to docetaxel when compared with EV controls (Figure 4K, right), in addition to inducing growth in the absence of hormones (charcoal stripped media) (Figure S4N). Of note, MASTL depletion significantly restored sensitivity to docetaxel in AR-V7-overexpressing cells (Figure S4O). Consistently, AR-V7 depletion induced a greater decrease in colony formation in 22Rv1-DR cells than in parental cells (Figure S4P) and re-sensitized DR cells to docetaxel (Figure S4Q). These results are in line with previous clinical studies[72,80,81] showing that AR-V7 expression at baseline is primarily linked to resistance to anti-androgen therapy, but also confers worse clinical outcomes in taxane-treated CRPC patients.

Finally, we assessed the clinical significance of the AR-V7/MASTL axis in metastatic PCa patients (SU2C)[6] and found that

---

Figure 3. Therapy-resistant lethal PCa exhibits a selective functional MASTL dependency to tolerate deleterious CIN

(A) Colony formation and quantifications comparing parental and DR cells after control or MASTL siRNAs.

(B) MASTL, total PARP, and cleaved PARP immunoblots in cells from (A), 72 h after siRNA.

(C) Colony formation and quantifications comparing parental and DR cells after control or MASTL CRISPR-Cas9-mediated knockout.

(D) MASTL, total PARP, and cleaved PARP immunoblots from cells in (C) 72 h after CRISPR-Cas9.

(E) Colony formation and quantifications of DR cells doxycycline-induced to express WT or KD (G44S, KD) FLAP-MASTL siRNA resistant (siR) compared with EV (FLAP) after control or MASTL siRNAs.

(F) MASTL and cleaved PARP immunoblots of cells from (E) after 72 h.

(G) Representative immunofluorescence images and quantifications of anaphases with lagging chromosomes comparing parental and DR cells after control or MASTL siRNAs. Centromeres (CREST), microtubules (alpha-tubulin). Red arrows point lagging chromosomes. Minimum of 100 cells scored per condition. *p ≤ 0.05, compares MASTL-depleted cells. **p ≤ 0.05, compares cells in siRNA control. Wilcoxon's test. Scale bar, 5 μm.

(H) Representative images and tumor weight quantification in parental/DR subcutaneous xenografts expressing control (n = 20) or two doxycycline-induced MASTL shRNAs (n = 10, each shRNA) for 28 days.

(I) Representative cleaved caspase-3 IHC images and quantification in same DR xenograft models as in (H) after 4 days of doxycycline. Unless indicated, data represent the mean ± standard deviation of at least three experiments. *p ≤ 0.05, determined by Student's t test. See also Figure S3 and Video S1.
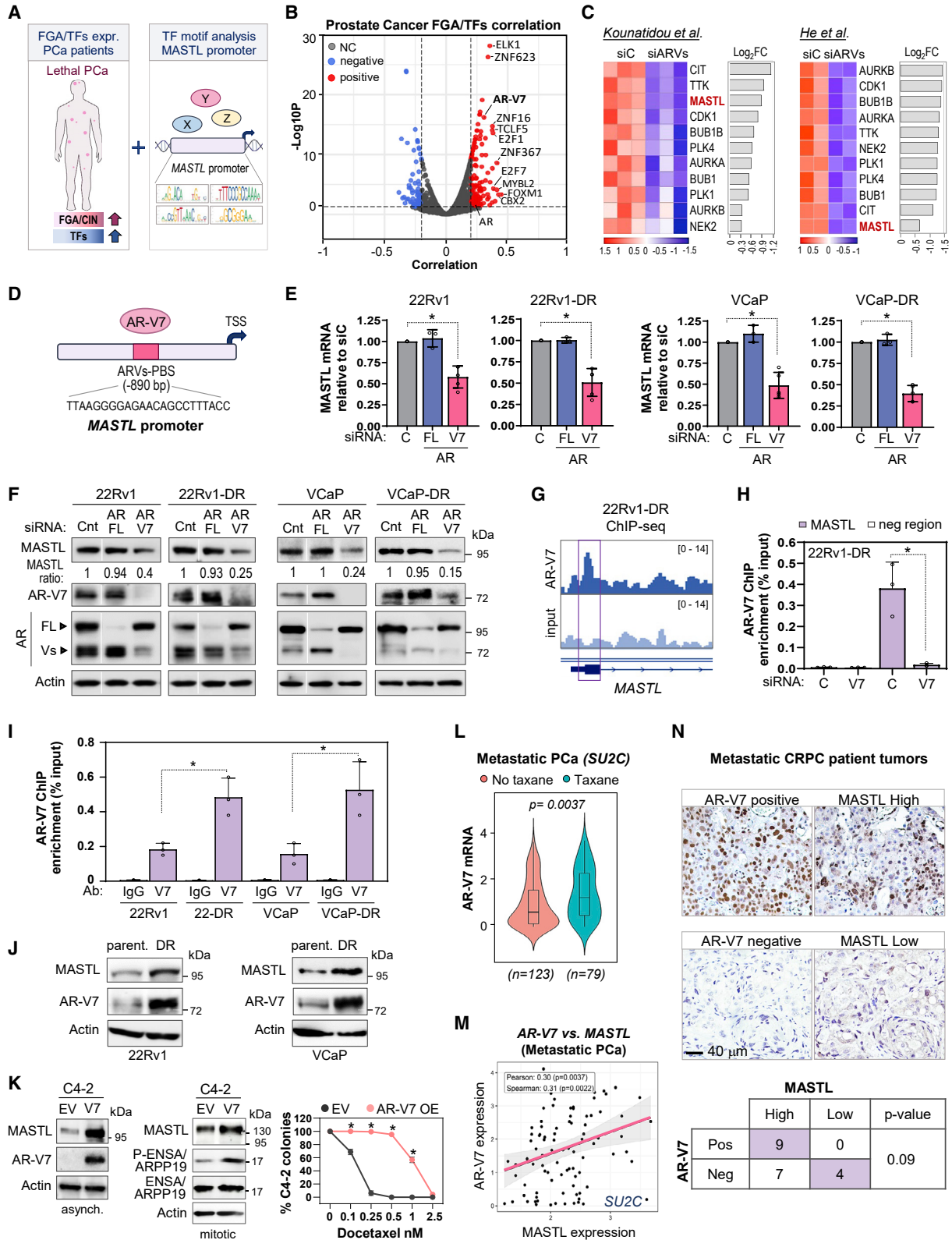
(legend on next page)

taxane-treated tumors display the highest AR-V7 expression (Figure 4L) and a positive correlation with MASTL mRNA expression that is non-existent with AR-FL (Figures 4M and S4R). This was confirmed at the protein level by IHC analysis of metastatic heavily treated PCa tissue samples (Figure 4N). Overall, our data indicate that AR-V7 expression plays a key role in the transcriptional upregulation of MASTL in high CIN therapy-refractory metastatic PCa and provides mechanistic insights on how AR-V7 may modulate taxane therapy response.

E2F7 transcriptionally regulates *MASTL* by direct promoter binding and through an AR-V7-dependent circuitry in therapy-resistant lethal PCa cells

Since MASTL is also upregulated in therapy-resistant cells that do not express AR-V7, we sought to determine additional mechanisms of transcriptional regulation. Our bioinformatic analysis had identified several E2F family members correlating with high FGA/CIN in PCa patient datasets, with E2F7 being the one with the strongest positive correlation (Figures 4B, S4B and Tables S5A and S5B). E2F7 has been shown to increase during PCa disease progression and to correlate with poor patient outcomes,[75] but its biological role remains unexplored. In addition, we identified an E2F7 binding motif 959 bp upstream of the *MASTL* TSS (Figure 5A), which prompted us to further investigate its function and potential role in *MASTL* transcriptional regulation in PCa. Like MASTL, E2F7 levels increase in metastatic PCa cells, being highest in DR models (Figures S5A and S5B), which also displayed lower colony formation after its depletion than parental cells (Figure S5C). Moreover, E2F7 knockdown (Figure S5D) reduced MASTL mRNA and protein levels in DR cells (Figures 5B and 5C) and in other AR-V7 negative cells (C4-2 and LNCaP) (Figure S5E). Subsequent ChIP-qPCR analysis confirmed E2F7 binding to the predicted element in the *MASTL* promoter, with greater enrichment in DR cells (Figures 5D, S5F and S5G). Functionally, E2F7 depletion induced chromosome segregation errors that were partially rescued by MASTL overexpression (Figure 5E), thus confirming a relevant role of the E2F7/MASTL axis in PCa cells chromosomal stability regulation. Of note, E2F1 and E2F8 also correlated with FGA/CIN in PCa patients (Figures 4B and S4B); however, their depletion

did not impact MASTL levels (Figures S5H–S5M), further confirming E2F7 as the main E2F regulating *MASTL* in PCa cells.

The clinical relevance of these findings was confirmed in multiple publicly available PCa patient datasets[1,6,63] in which E2F7/MASTL mRNA expression positively correlate (Figure 5F) and E2F7 shows increase expression in taxane-treated metastatic tumors (Figure 5G). These results were validated at the protein level by IHC in a cohort of PCa tissue samples (Figure 5H).

Because our data suggest that both AR-V7 and E2F7 can transcriptionally regulate *MASTL* in therapy-resistant PCa cells, we then investigated potential co-dependencies between both TFs. Analysis of the expression of each TF under knockdown conditions in 22Rv1-DR cells showed that AR-V7 regulates E2F7 expression (Figures S5N and S5O), while AR-V7 levels remain unchanged after E2F7 depletion (Figures S5P and S5Q). Conversely, the overexpression of AR-V7 in C4-2 cells upregulates both MASTL and E2F7 (Figure S5R), results that are in line with a previous report showing AR-V7 transcriptional regulation of E2F7.[75] These results indicate that AR-V7 can directly regulate MASTL gene expression by binding to its promoter and indirectly by transcriptionally upregulating E2F7 in PCa cells. Accordingly, the co-depletion of both TFs in 22Rv1-DR cells induced the greatest decrease in MASTL when compared with single TF knockdowns (Figure 5I), and the strongest decrease in colony formation in docetaxel-treated and untreated cells (Figure 5J). Collectively, our data suggest that elevated expression of atypical TFs like AR-V7 and E2F7 help to counteract deleterious CIN in therapy-refractory PCa.

Targeting MASTL induces deleterious CIN selectively in therapy refractory PCa cells

Our findings that MASTL upregulation promotes survival to deleterious CIN gave a rationale to exploit this vulnerability for potential therapeutic opportunities. To this end, we determined the efficacy of GKI-1, a first-generation small molecule MASTL inhibitor[52] not tested previously in PCa. GKI-1 treatment decreased the phosphorylation of MASTL targets ENSA and ARPP19, demonstrating efficient MASTL kinase inhibition in parental and DR cells (Figures 6A and S6A). Remarkably, MASTL inhibition decreased colony formation more efficiently in 22Rv1-DR and DU145-DR

Figure 4. AR-V7 transcriptionally regulates *MASTL* in lethal PCa

(A) Workflow of bioinformatic analysis of TFs enriched in high FGA/CIN PCa patients' tumors from publicly available datasets and *MASTL* promoter analysis of TF binding motifs.

(B) TFs/FGA correlation volcano plot of publicly available patient datasets.[2,6,63] NC, not correlated. $p \leq 0.05$ determined by Fisher z-transform.

(C) Transcriptomic heatmaps of mitotic kinases in control or ARVs depleted cells from two studies.[75,76] Red = high, blue = low.

(D) *MASTL* gene promoter diagram indicating ARVs-PBS binding motif location.

(E) MASTL mRNA levels after 48 h of control, AR-FL, or AR-V7 siRNA in parental and DR cells.

(F) Immunoblots of cells from (E) 72 h after siRNA. FL = full length; Vs = variants. Vertical white lines separate non-adjacent lanes in the original blot.

(G) AR-V7 ChIP-sequencing profile at the *MASTL* locus in 22Rv1-DR cells.

(H) AR-V7 ChIP-qPCR occupancy at the *MASTL* promoter in 22Rv1-DR cells. Flanking control region (neg region). Data relative to IgG control.

(I) AR-V7 ChIP-qPCR occupancy at *MASTL* promoter comparing parental and DR cells.

(J) MASTL and AR-V7 immunoblots comparing parental and DR cells.

(K) (Left) MASTL and AR-V7 immunoblots in control (EV) and overexpressing AR-V7 asynchronous C4-2 cells (asynch.). (Middle) MASTL, total and phospho-ENSA immunoblots in same cells in mitosis. (Right) Colony formation quantification of cells exposed to increasing concentrations of docetaxel for 72 h.

(L) AR-V7 mRNA levels in taxane-treated and naive metastatic PCa patient samples from the SU2C dataset.[6] p value determined by Wilcoxon's test.

(M) AR-V7 and MASTL gene expression correlation (Pearson/Spearman) in the SU2C dataset.[6]

(N) Representative IHC images and association between AR-V7 and MASTL protein expression in metastatic CRPC tissue samples (n = 20). p value determined by Fisher exact (χ^2 test) test. Unless indicated, data represent the mean ± standard deviation of at least three experiments. *$p \leq 0.05$, determined by Student's t test. See also Figure S4 and Tables S5A and S5B.
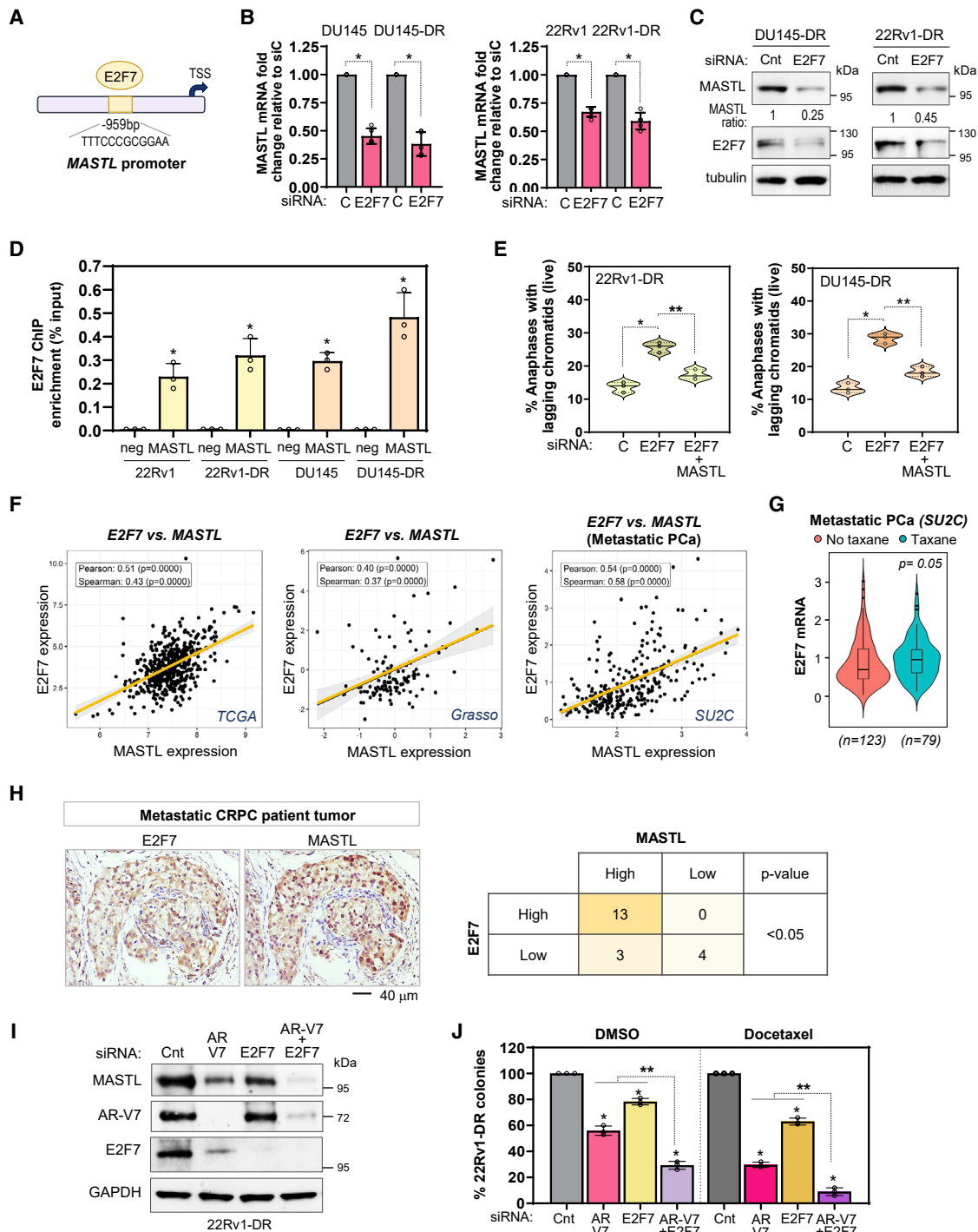
Figure 5. E2F7 restrains deleterious CIN by transcriptionally regulating *MASTL* in lethal PCa cells

(A) *MASTL* gene promoter diagram indicating the E2F7 binding motif location.

(B) MASTL mRNA levels after 48 h of control or E2F7 siRNA in parental and DR cells.

(C) Immunoblots of cells from (B), 72 h after siRNA.

(D) E2F7 ChIP-qPCR occupancy at the *MASTL* promoter in parental and DR cells. Flanking control region (neg). Data relative to IgG control.

(E) Quantification of percentage of anaphases with lagging chromosomes (live imaging) after control, E2F7 siRNAs alone or with MASTL overexpression in DR cells. A minimum of 100 cells/experiment scored. *p ≤ 0.05, comparing control and E2F7 siRNA. **p ≤ 0.05, comparing E2F7 siRNA with ot without MASTL overexpression.

(legend continued on next page)

cells than in syngenic parental cells (Figures 6B and S6B) and was associated with increased cell death (cleaved PARP) (Figure 6C). The lack of efficacy of GKI-1 in low MASTL-expressing cells was recapitulated in the LNCaP taxane-sensitive metastatic cell line model (Figure S6C). No further decrease in colony formation was seen after GKI-1 treatment of MASTL-depleted cells, suggesting the observed phenotypes were mainly due to MASTL inhibition and ruling out strong off target effects in our models (Figure S6D). Next, histone H2B-mCherry-expressing parental and DR cells treated with GKI-1 were subjected to live imaging to analyze effects on chromosome segregation. Notably, GKI-1 dramatically increased the number of anaphases with lagging chromosomes specifically in DR cells (Figure 6D), induced faster mitotic exit, and led to increases in other mitotic errors (micronuclei, multinucleated cells and multipolar spindles) (Figures S6E and S6F), all of them reminiscent of MASTL loss of function.

Since our data indicate that MASTL upregulation in metastatic therapy-refractory PCa cells confers sensitivity to MASTL targeting, we tested whether its overexpression in parental cells may render them more sensitive to MASTL inhibition. Indeed, induced MASTL upregulation in parental cells (Figure S6G) rendered them sensitive to GKI-1, as indicated by decreased colony formation and induced apoptosis (Figures 6E and 6F), mimicking the MASTL dependency of DR cells. In contrast, MASTL KD overexpression did not induce the same effects (Figures S6H–S6J), further confirming that increased MASTL activity confers sensitivity to GKI-1.

We next sought to determine whether MASTL inhibition could sensitize DR cells to standard therapy. Indeed, the combination of GKI-1 with docetaxel showed greater efficacy than each treatment alone in DR cells (Figure 6G). Of note, culturing metastatic hormone-sensitive PCa cells (VCaP) in androgen deprivation conditions (ADT), with charcoal-stripped media, induced a concomitant upregulation of AR-V7, E2F7, and MASTL and increased GKI-1 sensitivity (Figure 6H). Our results indicate that AR-V7/E2F7/MASTL upregulation is a common mechanism in castration and/or chemoresistant PCa cells, rendering them more sensitive to MASTL inhibition.

GKI-1 treatment increases survival of lethal PCa pre-clinical models bearing MASTL-addicted therapy-refractory tumors

We then sought to validate our results *in vivo* using cell line and patient-derived xenograft pre-clinical models. GKI-1 treatment in mice bearing subcutaneous parental and chemoresistant luciferase-tagged xenografts showed that DR tumors, which have greater MASTL expression (Figure S7A), had a significantly lower tumor photon flux and tumor weight after GKI-1 treatment (5 days/week for 28 days) than tumors derived from parental

cells (Figures 7A and S7B) without inducing general toxicity (Figure S7C). Remarkably, IHC analysis of treated tumors showed that GKI-1 efficacy was paralleled by an increase in chromosome segregation errors (Figure S7D) and higher apoptosis (cleaved Caspase 3 expression) (Figure 7B) in DR models. Moreover, when testing the efficacy of combining GKI-1 with standard therapy, we observed that mice bearing CRPC-DR xenografts treated with both GKI-1 and docetaxel displayed lower tumor weights when compared with vehicle and each treatment alone (Figure 7C). Similar results were observed when administering GKI-1 to castrated mice bearing hormone-sensitive VCaP xenografts (Figure 7D). Finally, we further validated these results in a cohort of four PCa patient-derived xenograft (PDX) models generated from circulating tumor cells of metastatic PCa patients[55,82] that had been previously treated with anti-androgen and/or taxane therapy (Figure S7E) and that express distinct levels of MASTL, AR-V7, and E2F7 (Figure 7E). Like observed with cell line xenografts, PDXs with elevated MASTL expression displayed higher GKI-1 sensitivity. High-MASTL models (PDX#2 and #4) had smaller tumor volumes (Figure 7F), higher count of lagging chromosomes (Figure 7G), increased cleaved PARP expression (Figure S7F), and higher overall mice survival than low-MASTL models (PDX#1 and #3) (Figure 7H). Remarkably, survival was significantly increased in mice bearing high-MASTL PDX models treated with the GKI-1 plus docetaxel combination (Figure 7I). Interestingly, a similar result was observed in a high-MASTL PDX model that partially responds to ADT (PDX#4), as the combination with GKI-1 significantly improved survival (Figure 7J). Overall, these studies suggest that targeting MASTL may translate into a valuable therapeutic strategy for high CIN metastatic therapy-refractory PCa.

DISCUSSION

Genomic abnormalities induced by CIN are pervasive events in cancers that correlate with advanced disease stages and higher aggressiveness by driving tumor evolution, metastases, and drug resistance.[27–34,38] In PCa, in which genome aberrations increase as a function of disease progression,[1,2,6,14–16,83] CIN and derived chromosomal errors have been associated with lethal disease,[19,46,47] but the mechanistic causes and consequences of CIN remain to be investigated. In this framework, here we uncovered that CIN is highest in castration chemotherapy-resistant metastatic PCa. The fact that therapy-refractory tumors continue growing despite the known CIN detrimental consequences for cells[25,4,39–42] suggests that PCa may develop adaptation mechanisms that remain to be identified. To date, exploiting genomic instability as a therapeutic strategy in advanced PCa has mainly focused on targeting DNA repair defects.[84–89] In contrast, CIN-targeting

---

(F) E2F7 and MASTL gene expression correlation (Pearson/Spearman) in publicly available PCa patient datasets.[1,6,63]

(G) E2F7 mRNA levels in taxane-treated and naive metastatic PCa patient samples from the SU2C dataset.[6] p value determined by Wilcoxon's test.

(H) Representative IHC images and association between E2F7 and MASTL protein expression in metastatic CRPC tissue samples (n = 20). p value determined by Fisher exact (χ^2 test) test.

(I) MASTL, AR-V7, and E2F7 immunoblots in 22Rv1-DR cells 72 h after single or combined depletion of AR-V7 and E2F7.

(J) Colony formation quantifications in cells from (I) exposed 72 h to DMSO or docetaxel (75 nM). *$p \leq 0.05$, compared with control. **$p \leq 0.05$, compared with combined AR-V7 + E2F7 with single siRNA. Unless indicated, data represent the mean ± standard deviation of at least three experiments. p values determined by Student's t test. See also Figure S5.
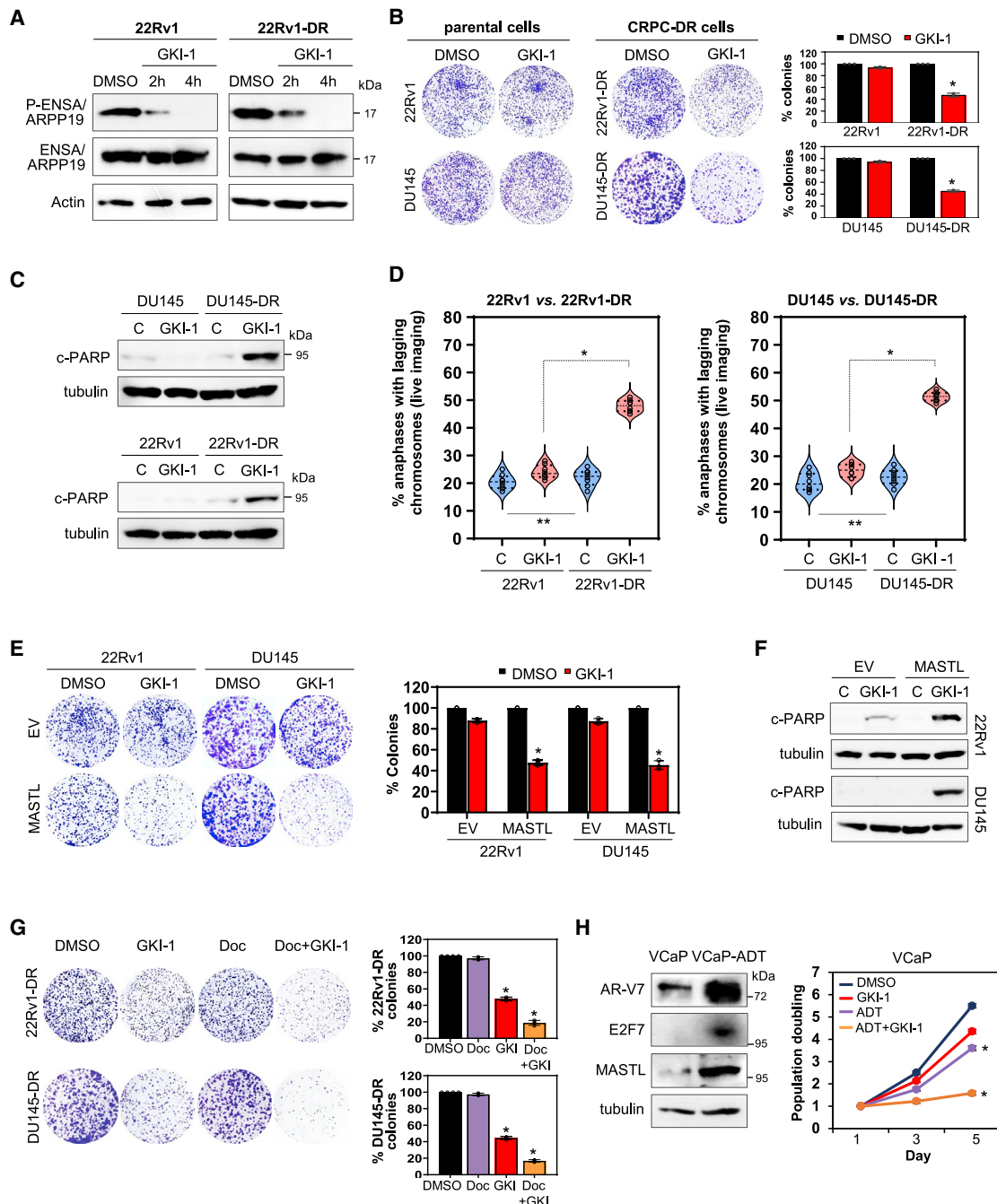
Figure 6. MASTL pharmacological inhibition selectively induces deleterious CIN in therapy-resistant PCa cells

(A) MASTL, total, and phospho-ENSA/ARPP19 immunoblots of mitotic parental and DR cells treated with 10 μM GKI-1 for 2 or 4 h.

(B) Colony formation and quantifications of DR/parental cells treated 72 h with control (DMSO) or 5 μM GKI-1.

(C) Immunoblots of cleaved PARP in cells from (B).

(D) Quantification of percentage of anaphases with lagging chromosomes (live imaging) in cells treated with 10 μM GKI-1. Minimum of 100 cells scored. *p ≤ 0.05, compares GKI-1-treated cells. **p ≤ 0.05, compares controls. p values determined by Wilcoxon's test.

(E) Colony formation and quantifications of parental cells expressing (EV) or MASTL overexpression treated with vehicle (DMSO) or 5 μM GKI-1 for 72 h.

(F) Immunoblots of cleaved PARP in cells from (E).

(G) Colony formation and quantifications of DR cells treated with DMSO, docetaxel (75 nM 22Rv1-DR or 250 nM DU145-DR), 5 μM GKI-1, or a combination.

(H) AR-V7, E2F7, and MASTL immunoblots in VCaP cells naive or grown 2 weeks in charcoal-stripped media (ADT). Right, population doubling of cells expose to vehicle (DMSO), 5 μM GKI-1, ADT, or a combination. Unless indicated, data represent the mean ± standard deviation of at least three experiments. *p ≤ 0.05, determined by Student's t test. See also Figure S6.
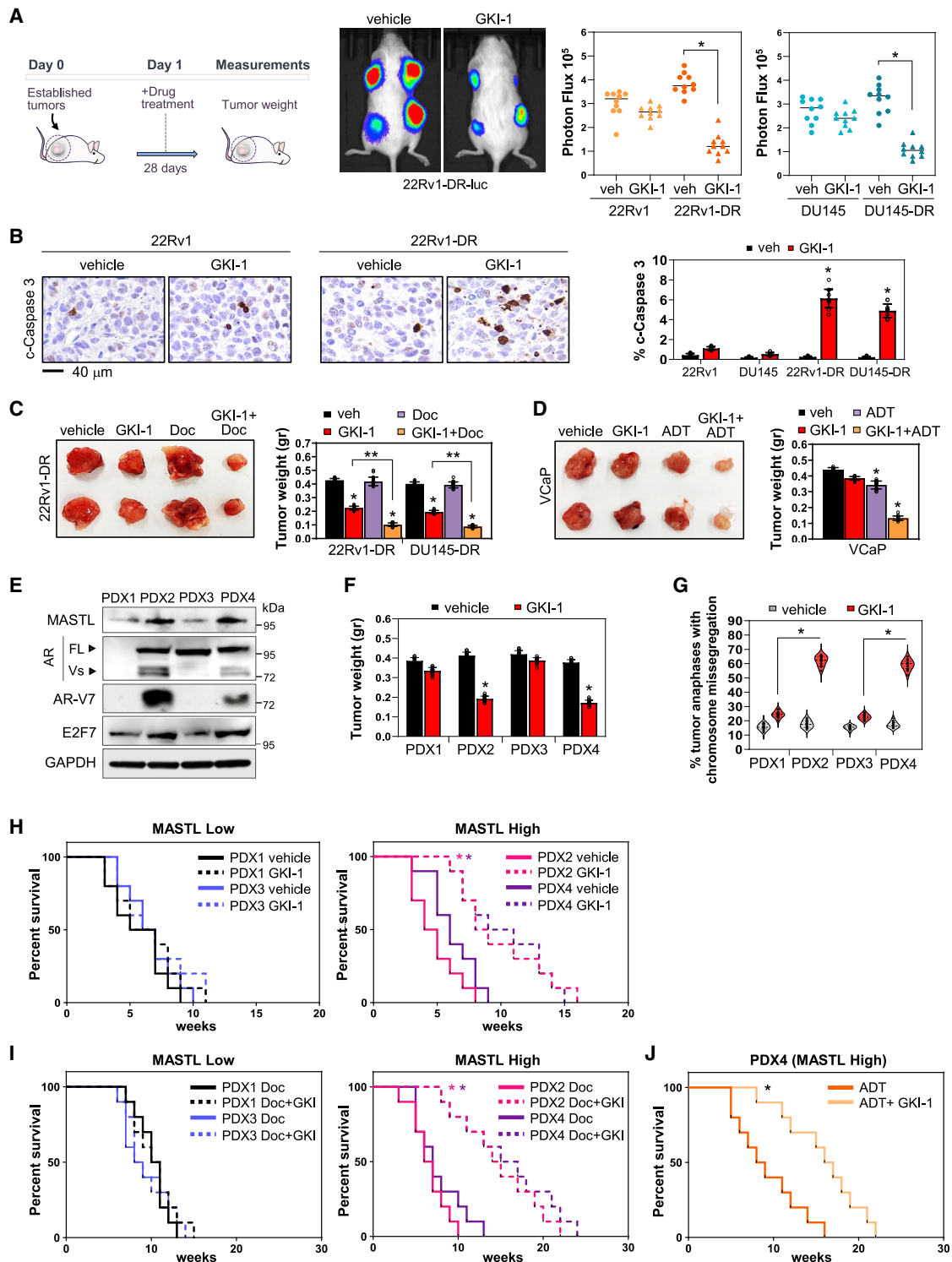
Figure 7. Targeting MASTL-dependent CIN tolerance *in vivo* increases survival of lethal PCa pre-clinical models

(A) Representative images and quantification of tumor photon flux bioluminescence of parental and DR luciferase-expressing xenografts in mice treated 28 days with vehicle (n = 10) or GKI-1 (n = 10).

(B) Cleaved caspase-3 IHC and quantification in xenografts of mice treated as in (A) for 4 days (n = 12 each group).

(C) Representative images and tumor weight quantification of DR subcutaneous xenografts of mice treated 28 days with vehicle, GKI-1, docetaxel or combinations. Twenty tumors per treatment condition were analyzed. *p ≤ 0.05; **p ≤ 0.05 in GKI-1 vs. GKI + Doc.

(legend continued on next page)

strategies are unexplored in PCa because the molecular underpinnings and consequences of CIN remain poorly understood. Of note, recent studies have shown that cells harboring aneuploidy or whole-genome doubling can be specifically targeted.[90,91] It is feasible to assume, then, that unveiling mechanisms underlying CIN tolerance in advanced PCa can turn a major force behind tumor progression into a source of tumor vulnerability that could be exploited therapeutically.

Here, we elucidated molecular and cellular processes allowing metastatic therapy-resistant PCa to tolerate and survive high CIN levels. Our findings indicate that metastatic tumors that had been treated with anti-androgen and chemotherapy (taxane) display increased FGA/CIN and mitotic fidelity kinase gene expression. Phosphoproteomic and functional analysis pinpointed a key role of MASTL as a top upregulated actionable kinase to which chemoresistant PCa cells become selectively addicted to survive by preventing the buildup of an extremely high burden of chromosomal aberrations. MASTL has an established role in regulating cell cycle and mitosis,[48,49,51] has been associated with cancer, and is proposed as a potential therapeutic target,[62,92–96] but the mechanisms underlying its deregulation and function in PCa remain unknown. Our data indicate that the selective sensitivity observed in MASTL-depleted or inhibited therapy-resistant PCa is due to elevation of CIN above a tolerable survival threshold. We uncovered that this is a functional dependency that transcriptionally can be driven by AR-V7, supporting previous reports proposing ARVs separate roles from full-length AR in modulating genome integrity genes.[68,75,76,97–101] Despite the recognized clinical relevance of AR-V7 in promoting resistance to anti-androgen therapy in metastatic PCa,[65–72,80] its biological functions have remained more elusive. In this context, our study uncovers a previously unknown function for AR-V7 in restraining deleterious CIN in therapy-resistant lethal PCa. From a clinical perspective, our data agree with previous studies showing that AR-V7-positive tumors correlate with poor patient response to anti-androgen therapy, but also with worse response to taxane therapy.[72,80,81] Thus, our work provides insight into an AR-V7-regulated mechanism promoting tumor survival to distinct standard therapies. Our findings also suggest that transcriptionally regulated CIN adaptation in PCa cells can be orchestrated by other TFs such as E2F7, which can also bind and regulate *MASTL* irrespective of AR-V7 expression. This confirms previous studies suggesting that atypical E2Fs can promote cancer aggressiveness in a context-dependent manner,[102–104] further supporting the proposed relevant role of E2Fs in regulating chromosomal stability in cancer[105–107] and opens the door to future studies to dissect transcriptional programs regulated by distinct atypical E2Fs. In addition to the role of AR-V7 and E2F7 alone, our data

indicate that they can cooperate to ensure CIN tolerance as part of a transcriptional circuitry in which AR-V7 can also transcriptionally upregulate E2F7. Altogether, our results support the far-reaching hypothesis that the expression of unconventional TFs confers a survival advantage to lethal PCa tumors accumulating CIN.

Finally, here we provide experimental proof of concept that the pharmacological inhibition of MASTL, as a strategy to induce tumor lethal CIN, increases the survival of mice bearing therapy-resistant high MASTL prostate tumors. Although we demonstrate MASTL on-target effects of GKI-1 in inducing deleterious CIN in cells, the future development of more potent and selective compounds is warranted to improve the therapeutic index of this treatment strategy. Still, our data indicate that the AR-V7/E2F7/MASTL axis may be a common molecular mechanism arising after exposure to different types of therapy and that combination of MASTL inhibition with standard therapy (ADT or docetaxel) significantly improves survival of patient-derived pre-clinical PCa models.

In summary, this study identified a mechanism of high CIN adaptation in metastatic therapy-resistant PCa. This functional dependency, mediated through AR-V7/E2F7 transcriptional rewiring and the upregulation of MASTL to avoid extreme CIN levels in metastatic cells, ensures tumor survival and progression. By targeting this vulnerability, we propose that CIN can be exploited as a therapeutic strategy for lethal PCa.

Limitations of the study

The methods used do not discern between structural and numerical CIN. Future studies should define causes and adaptation mechanisms of different CIN types in PCa considering diverse disease contexts, tumor genetic backgrounds, the status of genome integrity checkpoints, and mitotic error correction pathways in cell models and tumor samples. It is feasible that multiple mechanisms of CIN tolerance could cooperate, with MASTL upregulation being one of them. In addition, the specific downstream targets, and molecular mechanisms by which MASTL regulates chromosomal stability, remain to be elucidated to further understand implications in cancer.

STAR★METHODS

Detailed methods are provided in the online version of this paper and include the following:

- ● KEY RESOURCES TABLE
- ● RESOURCE AVAILABILITY
  - ○ Lead contact

(D) Representative images of VCaP subcutaneous xenografts of mice treated with vehicle, GKI-1, ADT (castration), or a combination for 28 days. Twenty tumors per treatment condition were analyzed.

(E) MASTL, AR, AR-V7, and E2F7 immunoblots in lethal PCa PDX models.

(F) Tumor weights from PDX models in mice treated 28 days with vehicle or GKI-1. Twenty tumors per treatment condition were analyzed.

(G) Percentage of anaphases with lagging chromosomes in PDX xenografts from mice treated for 4 days with vehicle or GKI-1 (n = 12 each group).

(H) Kaplan-Meier survival curves of mice intracardially injected with MASTL low or MASTL high PDX cells treated with vehicle or GKI-1.

(I) Kaplan-Meier survival curves of MASTL low or high PDX cells intracardially injected mice treated with docetaxel alone or with GKI-1.

(J) Kaplan-Meier survival curves of mice intracardially injected with MASTL high PDX4 cells treated with ADT (castration) or in combination with GKI-1. Vehicle, DMSO. GKI-1: 100 mg/kg/day i.p. Docetaxel: 10 mg/kg/weekly i.p. Unless indicated, p values determined by Student's t test.

(H–J) Ten mice for each treatment group analyzed. *p ≤ 0.05, log-rank test at the two-sided 0.05 level. See also Figure S7.

SUPPLEMENTAL INFORMATION

Supplemental information can be found online at https://doi.org/10.1016/j.xcrm.2023.100937.

AUTHOR CONTRIBUTIONS

Conceptualization, J.D.-D. and V.R.-B.; methodology, validation, investigation, and analysis, B.D., S.S., K.P., P.L., M.C.-C., M.X., A.E., J.D.-D., and V.R.-B; bioinformatics, A.E.; resources, pathology, clinical relevance, and pre-clinical work assistance, M.M., M.A.-F., A.L., J.L., C.N.S., M.J.S., W.K.K., C.C.-C., H.H., J.D.-D., and V.R.-B.; proteomic support, R.K.S., L.Z., and R.C.H.; writing draft with co-authors' input, V.R.-B.; draft review and editing, B.D., S.S., M.J.S., M.C.-C., J.D.-D., and V.R.-B.; research supervision, funding acquisition, and project administration, V.R.-B.

DECLARATION OF INTERESTS

The authors declare no competing financial interests.

INCLUSION AND DIVERSITY

One or more of the authors of this paper self-identifies as an under-represented ethnic minority in science, as a gender minority in their field of research and/or received support from a program designed to increase minority representation in science.

REFERENCES

1. Grasso, C.S., Wu, Y.M., Robinson, D.R., Cao, X., Dhanasekaran, S.M., Khan, A.P., Quist, M.J., Jing, X., Lonigro, R.J., Brenner, J.C., et al. (2012). The mutational landscape of lethal castration-resistant prostate cancer. Nature *487*, 239–243. https://doi.org/10.1038/nature11125.

2. Taylor, B.S., Schultz, N., Hieronymus, H., Gopalan, A., Xiao, Y., Carver, B.S., Arora, V.K., Kaushik, P., Cerami, E., Reva, B., et al. (2010). Integrative genomic profiling of human prostate cancer. Cancer Cell *18*, 11–22. https://doi.org/10.1016/j.ccr.2010.05.026.

3. Lapointe, J., Li, C., Giacomini, C.P., Salari, K., Huang, S., Wang, P., Ferrari, M., Hernandez-Boussard, T., Brooks, J.D., and Pollack, J.R. (2007). Genomic profiling reveals alternative genetic pathways of prostate tumorigenesis. Cancer Res. *67*, 8504–8510. https://doi.org/10.1158/0008-5472.Can-07-0673.

4. Birkbak, N.J., Eklund, A.C., Li, Q., McClelland, S.E., Endesfelder, D., Tan, P., Tan, I.B., Richardson, A.L., Szallasi, Z., and Swanton, C. (2011). Paradoxical relationship between chromosomal instability and survival outcome in cancer. Cancer Res. *71*, 3447–3452. https://doi.org/10.1158/0008-5472.can-10-3667.

5. Carter, S.L., Eklund, A.C., Kohane, I.S., Harris, L.N., and Szallasi, Z. (2006). A signature of chromosomal instability inferred from gene expression profiles predicts clinical outcome in multiple human cancers. Nat. Genet. *38*, 1043–1048. https://doi.org/10.1038/ng1861.

6. Abida, W., Cyrta, J., Heller, G., Prandi, D., Armenia, J., Coleman, I., Cieslik, M., Benelli, M., Robinson, D., Van Allen, E.M., et al. (2019). Genomic correlates of clinical outcome in advanced prostate cancer. Proc. Natl. Acad. Sci. USA *116*, 11428–11436. https://doi.org/10.1073/pnas.1902651116.

7. Sung, H., Ferlay, J., Siegel, R.L., Laversanne, M., Soerjomataram, I., Jemal, A., and Bray, F. (2021). Global cancer statistics 2020: GLOBOCAN estimates of incidence and mortality worldwide for 36 cancers in 185 countries. CA. Cancer J. Clin. *71*, 209–249. https://doi.org/10.3322/caac.21660.

8. Siegel, R.L., Miller, K.D., Fuchs, H.E., and Jemal, A. (2022). Cancer statistics, 2022. CA. Cancer J. Clin. *72*, 7–33. https://doi.org/10.3322/caac.21708.

9. Sumanasuriya, S., and De Bono, J. (2018). Treatment of advanced prostate cancer-A review of current therapies and future promise. Cold Spring Harb. Perspect. Med. *8*, a030635. https://doi.org/10.1101/cshperspect.a030635.

10. Rebello, R.J., Oing, C., Knudsen, K.E., Loeb, S., Johnson, D.C., Reiter, R.E., Gillessen, S., Van der Kwast, T., and Bristow, R.G. (2021). Prostate cancer. Nat. Rev. Dis. Primers *7*, 9. https://doi.org/10.1038/s41572-020-00243-0 (2021.

11. Carceles-Cordon, M., Kelly, W.K., Gomella, L., Knudsen, K.E., Rodriguez-Bravo, V., and Domingo-Domenech, J. (2020). Cellular rewiring in

lethal prostate cancer: the architect of drug resistance. Nat. Rev. Urol. *17*, 292–307. https://doi.org/10.1038/s41585-020-0298-8.

12. Beltran, H., Hruszkewycz, A., Scher, H.I., Hildesheim, J., Isaacs, J., Yu, E.Y., Kelly, K., Lin, D., Dicker, A., Arnold, J., et al. (2019). The role of lineage plasticity in prostate cancer therapy resistance. Clin. Cancer Res. *25*, 6916–6924. https://doi.org/10.1158/1078-0432.Ccr-19-1423.

13. Kumar, A., Coleman, I., Morrissey, C., Zhang, X., True, L.D., Gulati, R., Etzioni, R., Bolouri, H., Montgomery, B., White, T., et al. (2016). Substantial interindividual and limited intraindividual genomic diversity among tumors from men with metastatic prostate cancer. Nat. Med. *22*, 369–378. https://doi.org/10.1038/nm.4053.

14. Viswanathan, S.R., Ha, G., Hoff, A.M., Wala, J.A., Carrot-Zhang, J., Whelan, C.W., Haradhvala, N.J., Freeman, S.S., Reed, S.C., Rhoades, J., et al. (2018). Structural alterations driving castration-resistant prostate cancer revealed by linked-read genome sequencing. Cell *174*, 433–447.e19. https://doi.org/10.1016/j.cell.2018.05.036.

15. Quigley, D.A., Dang, H.X., Zhao, S.G., Lloyd, P., Aggarwal, R., Alumkal, J.J., Foye, A., Kothari, V., Perry, M.D., Bailey, A.M., et al. (2018). Genomic hallmarks and structural variation in metastatic prostate cancer. Cell *174*, 758–769.e9. https://doi.org/10.1016/j.cell.2018.06.039.

16. Robinson, D., Van Allen, E.M., Wu, Y.M., Schultz, N., Lonigro, R.J., Mosquera, J.M., Montgomery, B., Taplin, M.E., Pritchard, C.C., Attard, G., et al. (2015). Integrative clinical genomics of advanced prostate cancer. Cell *161*, 1215–1228. https://doi.org/10.1016/j.cell.2015.05.001.

17. Williams, J.L., Greer, P.A., and Squire, J.A. (2014). Recurrent copy number alterations in prostate cancer: an in silico meta-analysis of publicly available genomic data. Cancer Genet. *207*, 474–488. https://doi.org/10.1016/j.cancergen.2014.09.003.

18. Ryan, M.J., and Bose, R. (2019). Genomic alteration burden in advanced prostate cancer and therapeutic implications. Front. Oncol. *9*, 1287. https://doi.org/10.3389/fonc.2019.01287.

19. Nguyen, B., Fong, C., Luthra, A., Smith, S.A., DiNatale, R.G., Nandakumar, S., Walch, H., Chatila, W.K., Madupuri, R., Kundra, R., et al. (2022). Genomic characterization of metastatic patterns from prospective clinical sequencing of 25,000 patients. Cell *185*, 563–575.e11. https://doi.org/10.1016/j.cell.2022.01.003.

20. Armenia, J., Wankowicz, S.A.M., Liu, D., Gao, J., Kundra, R., Reznik, E., Chatila, W.K., Chakravarty, D., Han, G.C., Coleman, I., et al. (2018). The long tail of oncogenic drivers in prostate cancer. Nat. Genet. *50*, 645–651. https://doi.org/10.1038/s41588-018-0078-z.

21. Thompson, S.L., Bakhoum, S.F., and Compton, D.A. (2010). Mechanisms of chromosomal instability. Curr. Biol. *20*, R285–R295. https://doi.org/10.1016/j.cub.2010.01.034.

22. Levine, M.S., and Holland, A.J. (2018). The impact of mitotic errors on cell proliferation and tumorigenesis. Genes Dev. *32*, 620–638. https://doi.org/10.1101/gad.314351.118.

23. Bakhoum, S.F., and Swanton, C. (2014). Chromosomal instability, aneuploidy, and cancer. Front. Oncol. *4*, 161. https://doi.org/10.3389/fonc.2014.00161.

24. Rodriguez-Bravo, V., Maciejowski, J., Corona, J., Buch, H.K., Collin, P., Kanemaki, M.T., Shah, J.V., and Jallepalli, P.V. (2014). Nuclear pores protect genome integrity by assembling a premitotic and mad1-dependent anaphase inhibitor. Cell *156*, 1017–1031. https://doi.org/10.1016/j.cell.2014.01.010.

25. Gordon, D.J., Resio, B., and Pellman, D. (2012). Causes and consequences of aneuploidy in cancer. Nat. Rev. Genet. *13*, 189–203. https://doi.org/10.1038/nrg3123.

26. Kops, G.J.P.L., Weaver, B.A.A., and Cleveland, D.W. (2005). On the road to cancer: aneuploidy and the mitotic checkpoint. Nat. Rev. Cancer *5*, 773–785. https://doi.org/10.1038/nrc1714.

27. Lengauer, C., Kinzler, K.W., and Vogelstein, B. (1998). Genetic instabilities in human cancers. Nature *396*, 643–649. https://doi.org/10.1038/25292. https://www.nature.com/articles/25292#supplementary-information.

28. Boveri, T. (2008). Concerning the origin of malignant tumours by theodor boveri. Translated and annotated by henry harris. J. Cell Sci. *121*, 1–84. https://doi.org/10.1242/jcs.025742.

29. Thompson, S.L., and Compton, D.A. (2011). Chromosomes and cancer cells. Chromosome Res. *19*, 433–444. https://doi.org/10.1007/s10577-010-9179-y.

30. Sansregret, L., Vanhaesebroeck, B., and Swanton, C. (2018). Determinants and clinical implications of chromosomal instability in cancer. Nat. Rev. Clin. Oncol. *15*, 139–150. https://doi.org/10.1038/nrclinonc.2017.198.

31. Ben-David, U., and Amon, A. (2020). Context is everything: aneuploidy in cancer. Nat. Rev. Genet. *21*, 44–62. https://doi.org/10.1038/s41576-019-0171-x.

32. Bakhoum, S.F., Ngo, B., Laughney, A.M., Cavallo, J.A., Murphy, C.J., Ly, P., Shah, P., Sriram, R.K., Watkins, T.B.K., Taunk, N.K., et al. (2018). Chromosomal instability drives metastasis through a cytosolic DNA response. Nature *553*, 467–472. https://doi.org/10.1038/nature25432.

33. Sotillo, R., Hernando, E., Díaz-Rodríguez, E., Teruya-Feldstein, J., Cordón-Cardo, C., Lowe, S.W., and Benezra, R. (2007). Mad2 overexpression promotes aneuploidy and tumorigenesis in mice. Cancer Cell *11*, 9–23. https://doi.org/10.1016/j.ccr.2006.10.019.

34. Ippolito, M.R., Martis, V., Martin, S., Tijhuis, A.E., Hong, C., Wardenaar, R., Dumont, M., Zerbib, J., Spierings, D.C.J., Fachinetti, D., et al. (2021). Gene copy-number changes and chromosomal instability induced by aneuploidy confer resistance to chemotherapy. Dev. Cell *56*, 2440–2454.e6. https://doi.org/10.1016/j.devcel.2021.07.006.

35. Lee, A.J.X., Endesfelder, D., Rowan, A.J., Walther, A., Birkbak, N.J., Futreal, P.A., Downward, J., Szallasi, Z., Tomlinson, I.P.M., Howell, M., et al. (2011). Chromosomal instability confers intrinsic multidrug resistance. Cancer Res. *71*, 1858–1870. https://doi.org/10.1158/0008-5472.can-10-3604.

36. Swanton, C., Nicke, B., Schuett, M., Eklund, A.C., Ng, C., Li, Q., Hardcastle, T., Lee, A., Roy, R., East, P., et al. (2009). Chromosomal instability determines taxane response. Proc. Natl. Acad. Sci. USA *106*, 8671–8676. https://doi.org/10.1073/pnas.0811835106.

37. Watkins, T.B.K., Lim, E.L., Petkovic, M., Elizalde, S., Birkbak, N.J., Wilson, G.A., Moore, D.A., Grönroos, E., Rowan, A., Dewhurst, S.M., et al. (2020). Pervasive chromosomal instability and karyotype order in tumour evolution. Nature *587*, 126–132. https://doi.org/10.1038/s41586-020-2698-6.

38. Bakhoum, S.F., and Cantley, L.C. (2018). The multifaceted role of chromosomal instability in cancer and its microenvironment. Cell *174*, 1347–1360. https://doi.org/10.1016/j.cell.2018.08.027.

39. Torres, E.M., Williams, B.R., and Amon, A. (2008). Aneuploidy: cells losing their balance. Genetics *179*, 737–746. https://doi.org/10.1534/genetics.108.090878.

40. Pfau, S.J., and Amon, A. (2012). Chromosomal instability and aneuploidy in cancer: from yeast to man. EMBO Rep. *13*, 515–527. https://doi.org/10.1038/embor.2012.65.

41. Holland, A.J., and Cleveland, D.W. (2009). Boveri revisited: chromosomal instability, aneuploidy and tumorigenesis. Nat. Rev. Mol. Cell Biol. *10*, 478–487. https://doi.org/10.1038/nrm2718.

42. Torres, E.M., Sokolsky, T., Tucker, C.M., Chan, L.Y., Boselli, M., Dunham, M.J., and Amon, A. (2007). Effects of aneuploidy on cellular physiology and cell division in haploid yeast. Science *317*, 916–924. https://doi.org/10.1126/science.1142210.

43. Funk, L.C., Zasadil, L.M., and Weaver, B.A. (2016). Living in CIN: mitotic infidelity and its consequences for tumor promotion and suppression. Dev. Cell *39*, 638–652. https://doi.org/10.1016/j.devcel.2016.10.023.

44. Bakhoum, S.F., and Compton, D.A. (2012). Chromosomal instability and cancer: a complex relationship with therapeutic potential. J. Clin. Invest. *122*, 1138–1143. https://doi.org/10.1172/JCI59954.

45. Kops, G.J.P.L., Foltz, D.R., and Cleveland, D.W. (2004). Lethality to human cancer cells through massive chromosome loss by inhibition of the mitotic checkpoint. Proc. Natl. Acad. Sci. USA *101*, 8699–8704. https://doi.org/10.1073/pnas.0401142101.

46. Stopsack, K.H., Whittaker, C.A., Gerke, T.A., Loda, M., Kantoff, P.W., Mucci, L.A., and Amon, A. (2019). Aneuploidy drives lethal progression in prostate cancer. Proc. Natl. Acad. Sci. USA *116*, 11390–11395. https://doi.org/10.1073/pnas.1902645116.

47. Miller, E.T., You, S., Cadaneanu, R.M., Kim, M., Yoon, J., Liu, S.T., Li, X., Kwan, L., Hodge, J., Quist, M.J., et al. (2020). Chromosomal instability in untreated primary prostate cancer as an indicator of metastatic potential. BMC Cancer *20*, 398. https://doi.org/10.1186/s12885-020-06817-1.

48. Castro, A., and Lorca, T. (2018). Greatwall kinase at a glance. J. Cell Sci. *131*, jcs222364. https://doi.org/10.1242/jcs.222364.

49. Álvarez-Fernández, M., Sánchez-Martínez, R., Sanz-Castillo, B., Gan, P.P., Sanz-Flores, M., Trakala, M., Ruiz-Torres, M., Lorca, T., Castro, A., and Malumbres, M. (2013). Greatwall is essential to prevent mitotic collapse after nuclear envelope breakdown in mammals. Proc. Natl. Acad. Sci. USA *110*, 17374–17379. https://doi.org/10.1073/pnas.1310745110.

50. Charrasse, S., Gharbi-Ayachi, A., Burgess, A., Vera, J., Hached, K., Raynaud, P., Schwob, E., Lorca, T., and Castro, A. (2017). Ensa controls S-phase length by modulating Treslin levels. Nat. Commun. *8*, 206. https://doi.org/10.1038/s41467-017-00339-4.

51. Vigneron, S., Robert, P., Hached, K., Sundermann, L., Charrasse, S., Labbé, J.C., Castro, A., and Lorca, T. (2016). The master Greatwall kinase, a critical regulator of mitosis and meiosis. Int. J. Dev. Biol. *60*, 245–254. https://doi.org/10.1387/ijdb.160155tl.

52. Ocasio, C.A., Rajasekaran, M.B., Walker, S., Le Grand, D., Spencer, J., Pearl, F.M.G., Ward, S.E., Savic, V., Pearl, L.H., Hochegger, H., and Oliver, A.W. (2016). A first generation inhibitor of human Greatwall kinase, enabled by structural and functional characterisation of a minimal kinase domain construct. Oncotarget *7*, 71182–71197. https://doi.org/10.18632/oncotarget.11511.

53. Venkatesan, S., Angelova, M., Puttick, C., Zhai, H., Caswell, D.R., Lu, W.T., Dietzen, M., Galanos, P., Evangelou, K., Bellelli, R., et al. (2021). Induction of APOBEC3 exacerbates DNA replication stress and chromosomal instability in early breast and lung cancer evolution. Cancer Discov. *11*, 2456–2473. https://doi.org/10.1158/2159-8290.Cd-20-0725.

54. Domingo-Domenech, J., Vidal, S.J., Rodriguez-Bravo, V., Castillo-Martin, M., Quinn, S.A., Rodriguez-Barrueco, R., Bonal, D.M., Charytonowicz, E., Gladoun, N., de la Iglesia-Vicente, J., et al. (2012). Suppression of acquired docetaxel resistance in prostate cancer through depletion of notch- and hedgehog-dependent tumor-initiating cells. Cancer Cell *22*, 373–388. https://doi.org/10.1016/j.ccr.2012.07.016.

55. Vidal, S.J., Rodriguez-Bravo, V., Quinn, S.A., Rodriguez-Barrueco, R., Lujambio, A., Williams, E., Sun, X., de la Iglesia-Vicente, J., Lee, A., Readhead, B., et al. (2015). A targetable GATA2-IGF2 axis confers aggressiveness in lethal prostate cancer. Cancer Cell *27*, 223–239. https://doi.org/10.1016/j.ccell.2014.11.013.

56. Rodriguez-Bravo, V., Pippa, R., Song, W.M., Carceles-Cordon, M., Dominguez-Andres, A., Fujiwara, N., Woo, J., Koh, A.P., Ertel, A., Lokareddy, R.K., et al. (2018). Nuclear pores promote lethal prostate cancer by increasing POM121-driven E2F1, MYC, and AR nuclear import. Cell *174*, 1200–1215.e20. https://doi.org/10.1016/j.cell.2018.07.015.

57. Mohr, L., Carceles-Cordon, M., Woo, J., Cordon-Cardo, C., Domingo-Domenech, J., and Rodriguez-Bravo, V. (2017). Generation of prostate cancer cell models of resistance to the anti-mitotic agent docetaxel, p. e56327. https://doi.org/10.3791/56327.

58. Ong, S.E., Blagoev, B., Kratchmarova, I., Kristensen, D.B., Steen, H., Pandey, A., and Mann, M. (2002). Stable isotope labeling by amino acids in cell culture, SILAC, as a simple and accurate approach to expression proteomics. Mol. Cell. Proteomics *1*, 376–386. https://doi.org/10.1074/mcp.m200025-mcp200.

59. Reimand, J., Kull, M., Peterson, H., Hansen, J., and Vilo, J. (2007). Profiler–a web-based toolset for functional profiling of gene lists from large-scale experiments. Nucleic Acids Res. *35*, W193–W200. https://doi.org/10.1093/nar/gkm226.

60. Mochida, S., Maslen, S.L., Skehel, M., and Hunt, T. (2010). Greatwall phosphorylates an inhibitor of protein phosphatase 2A that is essential for mitosis. Science *330*, 1670–1673. https://doi.org/10.1126/science.1195689.

61. Gharbi-Ayachi, A., Labbé, J.C., Burgess, A., Vigneron, S., Strub, J.M., Brioudes, E., Van-Dorsselaer, A., Castro, A., and Lorca, T. (2010). The substrate of greatwall kinase, Arpp19, controls mitosis by inhibiting protein phosphatase 2A. Science *330*, 1673–1677. https://doi.org/10.1126/science.1197048.

62. Álvarez-Fernández, M., Sanz-Flores, M., Sanz-Castillo, B., Salazar-Roa, M., Partida, D., Zapatero-Solana, E., Ali, H.R., Manchado, E., Lowe, S., VanArsdale, T., et al. (2018). Therapeutic relevance of the PP2A-B55 inhibitory kinase MASTL/Greatwall in breast cancer. Cell Death Differ. *25*, 828–840. https://doi.org/10.1038/s41418-017-0024-0.

63. Cancer Genome Atlas Research Network (2015). The molecular taxonomy of primary prostate cancer. Cell *163*, 1011–1025. https://doi.org/10.1016/j.cell.2015.10.025.

64. Fornes, O., Castro-Mondragon, J.A., Khan, A., van der Lee, R., Zhang, X., Richmond, P.A., Modi, B.P., Correard, S., Gheorghe, M., Baranašić, D., et al. (2020). Jaspar 2020: update of the open-access database of transcription factor binding profiles. Nucleic Acids Res. *48*, D87-d92. https://doi.org/10.1093/nar/gkz1001.

65. Hu, R., Dunn, T.A., Wei, S., Isharwal, S., Veltri, R.W., Humphreys, E., Han, M., Partin, A.W., Vessella, R.L., Isaacs, W.B., et al. (2009). Ligand-independent androgen receptor variants derived from splicing of cryptic exons signify hormone-refractory prostate cancer. Cancer Res. *69*, 16–22. https://doi.org/10.1158/0008-5472.Can-08-2764.

66. Guo, Z., Yang, X., Sun, F., Jiang, R., Linn, D.E., Chen, H., Chen, H., Kong, X., Melamed, J., Tepper, C.G., et al. (2009). A novel androgen receptor splice variant is up-regulated during prostate cancer progression and promotes androgen depletion-resistant growth. Cancer Res. *69*, 2305–2313. https://doi.org/10.1158/0008-5472.Can-08-3795.

67. Chan, S.C., Li, Y., and Dehm, S.M. (2012). Androgen receptor splice variants activate androgen receptor target genes and support aberrant prostate cancer cell growth independent of canonical androgen receptor nuclear localization signal. J. Biol. Chem. *287*, 19736–19749. https://doi.org/10.1074/jbc.M112.352930.

68. Hu, R., Lu, C., Mostaghel, E.A., Yegnasubramanian, S., Gurel, M., Tannahill, C., Edwards, J., Isaacs, W.B., Nelson, P.S., Bluemn, E., et al. (2012). Distinct transcriptional programs mediated by the ligand-dependent full-length androgen receptor and its splice variants in castration-resistant prostate cancer. Cancer Res. *72*, 3457–3462. https://doi.org/10.1158/0008-5472.can-11-3892.

69. Li, Y., Chan, S.C., Brand, L.J., Hwang, T.H., Silverstein, K.A.T., and Dehm, S.M. (2013). Androgen receptor splice variants mediate enzalutamide resistance in castration-resistant prostate cancer cell lines. Cancer Res. *73*, 483–489. https://doi.org/10.1158/0008-5472.Can-12-3630.

70. Antonarakis, E.S., Lu, C., Wang, H., Luber, B., Nakazawa, M., Roeser, J.C., Chen, Y., Mohammad, T.A., Chen, Y., Fedor, H.L., et al. (2014). AR-V7 and resistance to enzalutamide and abiraterone in prostate cancer. N. Engl. J. Med. *371*, 1028–1038. https://doi.org/10.1056/NEJMoa1315815.

71. Antonarakis, E.S., Lu, C., Luber, B., Wang, H., Chen, Y., Zhu, Y., Silberstein, J.L., Taylor, M.N., Maughan, B.L., Denmeade, S.R., et al. (2017). Clinical significance of androgen receptor splice variant-7 mRNA detection in circulating tumor cells of men with metastatic castration-resistant prostate cancer treated with first- and second-line abiraterone and enzalutamide. J. Clin. Oncol. *35*, 2149–2156. https://doi.org/10.1200/JCO.2016.70.1961.

72. Sharp, A., Coleman, I., Yuan, W., Sprenger, C., Dolling, D., Rodrigues, D.N., Russo, J.W., Figueiredo, I., Bertan, C., Seed, G., et al. (2019).

Androgen receptor splice variant-7 expression emerges with castration resistance in prostate cancer. J. Clin. Invest. *129*, 192–208. https://doi.org/10.1172/JCI122819.

73. Luo, J., Attard, G., Balk, S.P., Bevan, C., Burnstein, K., Cato, L., Cherkasov, A., De Bono, J.S., Dong, Y., Gao, A.C., et al. (2018). Role of androgen receptor variants in prostate cancer: report from the 2017 mission androgen receptor variants meeting. Eur. Urol. *73*, 715–723. https://doi.org/10.1016/j.eururo.2017.11.038.

74. Balk, S.P., and Knudsen, K.E. (2008). The cell cycle, and prostate cancer. Nucl. Recept. Signal. *6*, e001. https://doi.org/10.1621/nrs.06001.

75. He, Y., Lu, J., Ye, Z., Hao, S., Wang, L., Kohli, M., Tindall, D.J., Li, B., Zhu, R., Wang, L., and Huang, H. (2018). Androgen receptor splice variants bind to constitutively open chromatin and promote abiraterone-resistant growth of prostate cancer. Nucleic Acids Res. *46*, 1895–1911. https://doi.org/10.1093/nar/gkx1306.

76. Kounatidou, E., Nakjang, S., McCracken, S.R.C., Dehm, S.M., Robson, C.N., Jones, D., and Gaughan, L. (2019). A novel CRISPR-engineered prostate cancer cell line defines the AR-V transcriptome and identifies PARP inhibitor sensitivities. Nucleic Acids Res. *47*, 5634–5647. https://doi.org/10.1093/nar/gkz286.

77. Cai, L., Tsai, Y.H., Wang, P., Wang, J., Li, D., Fan, H., Zhao, Y., Bareja, R., Lu, R., Wilson, E.M., et al. (2018). ZFX mediates non-canonical oncogenic functions of the androgen receptor splice variant 7 in castrate-resistant prostate cancer. Mol. Cell *72*, 341–354.e6. https://doi.org/10.1016/j.molcel.2018.08.029.

78. Cato, L., de Tribolet-Hardy, J., Lee, I., Rottenberg, J.T., Coleman, I., Melchers, D., Houtman, R., Xiao, T., Li, W., Uo, T., et al. (2019). ARv7 represses tumor-suppressor genes in castration-resistant prostate cancer. Cancer Cell *35*, 401–413.e6. https://doi.org/10.1016/j.ccell.2019.01.008.

79. Chen, Z., Wu, D., Thomas-Ahner, J.M., Lu, C., Zhao, P., Zhang, Q., Geraghty, C., Yan, P.S., Hankey, W., Sunkel, B., et al. (2018). Diverse AR-V7 cistromes in castration-resistant prostate cancer are governed by HoxB13. Proc. Natl. Acad. Sci. USA *115*, 6810–6815. https://doi.org/10.1073/pnas.1718811115.

80. Scher, H.I., Lu, D., Schreiber, N.A., Louw, J., Graf, R.P., Vargas, H.A., Johnson, A., Jendrisak, A., Bambury, R., Danila, D., et al. (2016). Association of AR-V7 on circulating tumor cells as a treatment-specific biomarker with outcomes and survival in castration-resistant prostate cancer. JAMA Oncol. *2*, 1441–1449. https://doi.org/10.1001/jamaoncol.2016.1828.

81. Marín-Aguilera, M., et al. (2020). Androgen receptor and its splicing variant 7 expression in peripheral blood mononuclear cells and in circulating tumor cells in metastatic castration-resistant prostate cancer. Cells *9*. https://doi.org/10.3390/cells9010203.

82. Williams, E.S., Rodriquez-Bravo, V., Chippada-Venkata, U., De la Iglesia-Vicente, J., Gong, Y., Galsky, M., Oh, W., Cordon-Cardo, C., and Domingo-Domenech, J. (2015). Generation of prostate cancer patient derived xenograft models from circulating tumor cells. J. Vis. Exp., 53182. https://doi.org/10.3791/53182.

83. Baca, S.C., Prandi, D., Lawrence, M.S., Mosquera, J.M., Romanel, A., Drier, Y., Park, K., Kitabayashi, N., MacDonald, T.Y., Ghandi, M., et al. (2013). Punctuated evolution of prostate cancer genomes. Cell *153*, 666–677. https://doi.org/10.1016/j.cell.2013.03.021.

84. Pritchard, C.C., Mateo, J., Walsh, M.F., De Sarkar, N., Abida, W., Beltran, H., Garofalo, A., Gulati, R., Carreira, S., Eeles, R., et al. (2016). Inherited DNA-repair gene mutations in men with metastatic prostate cancer. N. Engl. J. Med. *375*, 443–453. https://doi.org/10.1056/NEJMoa1603144.

85. Mateo, J., Carreira, S., Sandhu, S., Miranda, S., Mossop, H., Perez-Lopez, R., Nava Rodrigues, D., Robinson, D., Omlin, A., Tunariu, N., et al. (2015). DNA-repair defects and olaparib in metastatic prostate cancer. N. Engl. J. Med. *373*, 1697–1708. https://doi.org/10.1056/NEJMoa1506859.

86. Neeb, A., Herranz, N., Arce-Gallego, S., Miranda, S., Buroni, L., Yuan, W., Athie, A., Casals, T., Carmichael, J., Rodrigues, D.N., et al. (2021). Advanced prostate cancer with ATM loss: PARP and ATR inhibitors. Eur. Urol. *79*, 200–211. https://doi.org/10.1016/j.eururo.2020.10.029.

87. Mateo, J., Boysen, G., Barbieri, C.E., Bryant, H.E., Castro, E., Nelson, P.S., Olmos, D., Pritchard, C.C., Rubin, M.A., and de Bono, J.S. (2017). DNA repair in prostate cancer: biology and clinical implications. Eur. Urol. *71*, 417–425. https://doi.org/10.1016/j.eururo.2016.08.037.

88. de Bono, J., Mateo, J., Fizazi, K., Saad, F., Shore, N., Sandhu, S., Chi, K.N., Sartor, O., Agarwal, N., Olmos, D., et al. (2020). Olaparib for metastatic castration-resistant prostate cancer. N. Engl. J. Med. *382*, 2091–2102. https://doi.org/10.1056/NEJMoa1911440.

89. Rafiei, S., Fitzpatrick, K., Liu, D., Cai, M.Y., Elmarakeby, H.A., Park, J., Ricker, C., Kochupurakkal, B.S., Choudhury, A.D., Hahn, W.C., et al. (2020). ATM loss confers greater sensitivity to ATR inhibition than PARP inhibition in prostate cancer. Cancer Res. *80*, 2094–2100. https://doi.org/10.1158/0008-5472.Can-19-3126.

90. Quinton, R.J., DiDomizio, A., Vittoria, M.A., Kotýnková, K., Ticas, C.J., Patel, S., Koga, Y., Vakhshoorzadeh, J., Hermance, N., Kuroda, T.S., et al. (2021). Whole-genome doubling confers unique genetic vulnerabilities on tumour cells. Nature *590*, 492–497. https://doi.org/10.1038/s41586-020-03133-3.

91. Cohen-Sharir, Y., McFarland, J.M., Abdusamad, M., Marquis, C., Bernhard, S.V., Kazachkova, M., Tang, H., Ippolito, M.R., Laue, K., Zerbib, J., et al. (2021). Aneuploidy renders cancer cells vulnerable to mitotic checkpoint inhibition. Nature *590*, 486–491. https://doi.org/10.1038/s41586-020-03114-6 (2021.

92. Wang, L., Luong, V.Q., Giannini, P.J., and Peng, A. (2014). Mastl kinase, a promising therapeutic target, promotes cancer recurrence. Oncotarget *5*, 11479–11489. https://doi.org/10.18632/oncotarget.2565.

93. Yoon, Y.N., Choe, M.H., Jung, K.Y., Hwang, S.G., Oh, J.S., and Kim, J.S. (2018). MASTL inhibition promotes mitotic catastrophe through PP2A activation to inhibit cancer growth and radioresistance in breast cancer cells. BMC Cancer *18*, 716. https://doi.org/10.1186/s12885-018-4600-6.

94. Rogers, S., McCloy, R.A., Parker, B.L., Gallego-Ortega, D., Law, A.M.K., Chin, V.T., Conway, J.R.W., Fey, D., Millar, E.K.A., O'Toole, S., et al. (2018). MASTL overexpression promotes chromosome instability and metastasis in breast cancer. Oncogene *37*, 4518–4533. https://doi.org/10.1038/s41388-018-0295-z.

95. Marzec, K., and Burgess, A. (2018). The oncogenic functions of MASTL kinase. Front. Cell Dev. Biol. *6*, 162.

96. Fatima, I., Barman, S., Uppada, J., Chauhan, S., Rauth, S., Rachagani, S., Ponnusamy, M.P., Smith, L., Talmon, G., Singh, A.B., et al. (2021). MASTL regulates EGFR signaling to impact pancreatic cancer progression. Oncogene *40*, 5691–5704. https://doi.org/10.1038/s41388-021-01951-x (2021.

97. Ware, K.E., Garcia-Blanco, M.A., Armstrong, A.J., and Dehm, S.M. (2014). Biologic and clinical significance of androgen receptor variants in castration resistant prostate cancer. Endocr. Relat. Cancer *21*, T87-t103. https://doi.org/10.1530/erc-13-0470.

98. Roggero, C.M., Jin, L., Cao, S., Sonavane, R., Kopplin, N.G., Ta, H.Q., Ekoue, D.N., Witwer, M., Ma, S., Liu, H., et al. (2021). A detailed characterization of stepwise activation of the androgen receptor variant 7 in prostate cancer cells. Oncogene *40*, 1106–1117. https://doi.org/10.1038/s41388-020-01585-5.

99. Liang, J., Wang, L., Poluben, L., Nouri, M., Arai, S., Xie, L., Voznesensky, O.S., Cato, L., Yuan, X., Russo, J.W., et al. (2021). Androgen receptor splice variant 7 functions independently of the full length receptor in prostate cancer cells. Cancer Lett. *519*, 172–184. https://doi.org/10.1016/j.canlet.2021.07.013.

100. Magani, F., Bray, E.R., Martinez, M.J., Zhao, N., Copello, V.A., Heidman, L., Peacock, S.O., Wiley, D.J., D'Urso, G., and Burnstein, K.L. (2018). Identification of an oncogenic network with prognostic and therapeutic value in prostate cancer. Mol. Syst. Biol. *14*, e8202. https://doi.org/10.15252/msb.20188202.

101. Zhao, N., Peacock, S.O., Lo, C.H., Heidman, L.M., Rice, M.A., Fahrenholtz, C.D., Greene, A.M., Magani, F., Copello, V.A., Martinez, M.J., et al. (2019). Arginine vasopressin receptor 1a is a therapeutic target for castration-resistant prostate cancer. Sci. Transl. Med. *11*, eaaw4636. https://doi.org/10.1126/scitranslmed.aaw4636.

102. Moreno, E., Pandit, S.K., Toussaint, M.J.M., Bongiovanni, L., Harkema, L., van Essen, S.C., van Liere, E.A., Westendorp, B., and de Bruin, A. (2021). Atypical E2Fs either counteract or cooperate with RB during tumorigenesis depending on tissue context. Cancers *13*, 2033. https://doi.org/10.3390/cancers13092033.

103. Tian, J., Lin, Y., and Yu, J. (2017). E2F8 confers cisplatin resistance to ER+ breast cancer cells via transcriptionally activating MASTL. Biomed. Pharmacother. *92*, 919–926. https://doi.org/10.1016/j.biopha.2017.05.118.

104. Weijts, B.G.M.W., Bakker, W.J., Cornelissen, P.W.A., Liang, K.H., Schaftenaar, F.H., Westendorp, B., de Wolf, C.A.C.M.T., Paciejewska, M., Scheele, C.L.G.J., Kent, L., et al. (2012). E2F7 and E2F8 promote angiogenesis through transcriptional activation of VEGFA in cooperation with HIF1. Embo j *31*, 3871–3884. https://doi.org/10.1038/emboj.2012.231.

105. Dimova, D.K., and Dyson, N.J. (2005). The E2F transcriptional network: old acquaintances with new faces. Oncogene *24*, 2810–2826. https://doi.org/10.1038/sj.onc.1208612.

106. Chen, H.Z., Tsai, S.Y., and Leone, G. (2009). Emerging roles of E2Fs in cancer: an exit from cell cycle control. Nat. Rev. Cancer *9*, 785–797. https://doi.org/10.1038/nrc2696.

107. Pfister, K., Pipka, J.L., Chiang, C., Liu, Y., Clark, R.A., Keller, R., Skoglund, P., Guertin, M.J., Hall, I.M., and Stukenberg, P.T. (2018). Identification of drivers of aneuploidy in breast tumors. Cell Rep. *23*, 2758–2769. https://doi.org/10.1016/j.celrep.2018.04.102.

108. Cox, J., and Mann, M. (2008). MaxQuant enables high peptide identification rates, individualized p.p.b.-range mass accuracies and proteome-wide protein quantification. Nat. Biotechnol. *26*, 1367–1372. https://doi.org/10.1038/nbt.1511.

109. Robinson, M.D., McCarthy, D.J., and Smyth, G.K. (2010). edgeR: a Bioconductor package for differential expression analysis of digital gene expression data. Bioinformatics *26*, 139–140. https://doi.org/10.1093/bioinformatics/btp616.

110. Hänzelmann, S., Castelo, R., and Guinney, J. (2013). Gene set variation analysis for microarray and RNA-Seq data. BMC Bioinf. *14*, 7. https://doi.org/10.1186/1471-2105-14-7.

111. Fellmann, C., Zuber, J., McJunkin, K., Chang, K., Malone, C.D., Dickins, R.A., Xu, Q., Hengartner, M.O., Elledge, S.J., Hannon, G.J., and Lowe, S.W. (2011). Functional identification of optimized RNAi triggers using a massively parallel sensor assay. Mol. Cell *41*, 733–746. https://doi.org/10.1016/j.molcel.2011.02.008.

112. Villén, J., and Gygi, S.P. (2008). The SCX/IMAC enrichment approach for global phosphorylation analysis by mass spectrometry. Nat. Protoc. *3*, 1630–1638. https://doi.org/10.1038/nprot.2008.150.

113. Olsen, J.V., Blagoev, B., Gnad, F., Macek, B., Kumar, C., Mortensen, P., and Mann, M. (2006). Global, in vivo, and site-specific phosphorylation dynamics in signaling networks. Cell *127*, 635–648. https://doi.org/10.1016/j.cell.2006.09.026.

114. Olsen, J.V., Vermeulen, M., Santamaria, A., Kumar, C., Miller, M.L., Jensen, L.J., Gnad, F., Cox, J., Jensen, T.S., Nigg, E.A., et al. (2010). Quantitative phosphoproteomics reveals widespread full phosphorylation site occupancy during mitosis. Sci. Signal. *3*, ra3. https://doi.org/10.1126/scisignal.2000475.

115. Vizcaíno, J.A., Deutsch, E.W., Wang, R., Csordas, A., Reisinger, F., Ríos, D., Dianes, J.A., Sun, Z., Farrah, T., Bandeira, N., et al. (2014). ProteomeXchange provides globally coordinated proteomics data submission and dissemination. Nat. Biotechnol. *32*, 223–226. https://doi.org/10.1038/nbt.2839.

116. Lambert, S.A., Jolma, A., Campitelli, L.F., Das, P.K., Yin, Y., Albu, M., Chen, X., Taipale, J., Hughes, T.R., and Weirauch, M.T. (2018). The human transcription factors. Cell *172*, 650–665. https://doi.org/10.1016/j.cell.2018.01.029.

117. Schwarzer, G., Carpenter, J.R., and Rücker, G. (2015). Meta-analysis with R*4784* (Springer).

118. Cerami, E., Gao, J., Dogrusoz, U., Gross, B.E., Sumer, S.O., Aksoy, B.A., Jacobsen, A., Byrne, C.J., Heuer, M.L., Larsson, E., et al. (2012). The cBio cancer genomics portal: an open platform for exploring multidimensional cancer genomics data. Cancer Discov. *2*, 401–404. https://doi.org/10.1158/2159-8290.Cd-12-0095.

119. Li, H., and Durbin, R. (2010). Fast and accurate long-read alignment with Burrows–Wheeler transform. Bioinformatics *26*, 589–595. https://doi.org/10.1093/bioinformatics/btp698.

120. Zhang, Y., Liu, T., Meyer, C.A., Eeckhoute, J., Johnson, D.S., Bernstein, B.E., Nusbaum, C., Myers, R.M., Brown, M., Li, W., and Liu, X.S. (2008). Model-based analysis of ChIP-seq (MACS). Genome Biol. *9*, R137. https://doi.org/10.1186/gb-2008-9-9-r137.

121. Campbell, J.P., Merkel, A.R., Masood-Campbell, S.K., Elefteriou, F., and Sterling, J.A. (2012). Models of bone metastasis. J. Vis. Exp., e4260. https://doi.org/10.3791/4260.

STAR★METHODS

KEY RESOURCES TABLE

REAGENT or RESOURCE	SOURCE	IDENTIFIER
Antibodies		
Mouse anti-MASTL (4F9) (WB)	Millipore	Cat# MABT372
Rabbit anti-MASTL (IHC)	Abcam	Cat# ab86387; RRID:AB1925198
Rabbit anti-phospho-ENSA (Ser67)/ARPP19 (Ser62)	Cell Signaling	Cat# 5240; RRID:AB11220425
Rabbit polyclonal anti-ENSA	Cell Signaling	Cat# 8770; RRID:AB11217626
Rabbit anti-phospho-Histone H3 (S10)	Cell Signaling	Cat# 9701; RRID:AB331535
CREST auto-immune antibodies (human)	Immunovision	Cat# HCT-0100; RRID:AB2744669
Mouse anti-tubulin (DM1a) FITC conjugated (IF)	Sigma-Aldrich	Cat# T9026; RRID:AB477593
Rabbit anti-cleaved PARP (Asp214) (D64E10)	Cell Signaling	Cat# 5625; RRID:AB10699459
Rabbit anti total PARP (46D11)	Cell Signaling	Cat# 9532; RRID:AB659884
Rabbit anti-cleaved caspase-3	Cell Signaling	Cat# 9661; RRID:AB2341188
Rabbit anti-Androgen Receptor (AR) (WB)	Abcam	Cat# ab133273; RRID:AB11156085
Rabbit anti-Androgen Receptor (AR) (N-20) (ChIP)	Santa Cruz	Cat# sc-816; RRID:AB1563391
Rabbit anti-Androgen Receptor, AR-V7 specific (WB)	Abcam	Cat# ab198394, RRID:AB2861275
Mouse anti-AR-V7 specific (ChIP)	Precision	Cat# AG10008; RRID:AB2631057
Rabbit anti-Androgen Receptor, AR-V7 specific Clone RM7 (IHC)	RevMAb Biosciences	Cat# 31-1109-00; RRID:AB2716436
Rabbit anti-E2F7 (ChIP)	Abcam	Cat# ab56022; RRID:AB880024
Rabbit anti-E2F7 (ChIP)	Abcam	Cat# ab245655
Rabbit anti-E2F7 (WB, IHC)	ThermoFisher	Cat# PA5-68911; RRID:AB2688627
Rabbit anti-E2F8 (WB)	Bethyl	Cat# A303-039A; RRID:AB2615478
Rabbit monoclonal anti-E2F1 (WB)	Abcam	Cat# ab179445
Mouse monoclonal anti-Tubulin α (DM1A)	Millipore	Cat# CP06; RRID:AB2617116
Mouse anti-β-Actin	Sigma	Cat# A5441; RRID:AB476744
Rabbit anti-GAPDH antibody [EPR16891]	Abcam	Cat# ab181602; RRID:AB2630358
Anti-mouse Ig, Horseradish Peroxidase	Cytiva	Cat# NA931; RRID:AB772210
Anti-Rabbit Ig, Horseradish Peroxidase	Cytiva	Cat# NA934; RRID:AB772206
Alexa Fluor® 488 AffiniPure Donkey anti-Mouse IgG (H + L)	Jackson ImmunoResearch	Cat# 715-545-150; RRID:AB2340846
Alexa Fluor® 647 AffiniPure Donkey anti-Human IgG (H + L)	Jackson ImmunoResearch	Cat# 709-605-149; RRID:AB2340578
Rhodamine (TRITC) AffiniPure Donkey anti-Rabbit IgG (H + L)	Jackson ImmunoResearch	Cat# 711-025-152; RRID:AB2340588
Normal Rabbit IgG antibody	Cell Signaling	Cat# 2729; RRID:AB1031062
Normal Mouse IgG antibody	Jackson ImmunoResearch	Cat# 015-000-002; RRID:AB2337187
Bacterial and virus strains		
NEB 5-alpha competent E. Coli	New England Biolabs	Cat# C2987H
One Shot™ Stbl3™ Chemically Competent *E. coli*	ThermoFisher	Cat# C737303
Biological samples		
Prostate cancer paraffin embedded tumor samples	Mount Sinai Medical Center and CHTN	N/A (see STAR Methods section for details)
Chemicals, peptides, and recombinant proteins		
Docetaxel	Selleck Chemicals	Cat# S1148
Nocodazole	Selleck Chemicals	Cat# S2775
MG132	Cayman Chemical	Cat# 13697

(Continued on next page)

Continued

REAGENT or RESOURCE	SOURCE	IDENTIFIER
GKI-1	MedChemExpress	Cat# HY-100521
Geneticin (G418 sulfate)	Gibco	Cat# 10131027
Doxycycline hyclate	MilliporeSigma	Cat# 324385
Blasticidin S HCl	Gibco	Cat# A1113903
Puromycin Dihydrochloride	Gibco	Cat# A1113803
Monastrol	Selleck Chemical LLC	Cat# 329689-23-8
ProLong™ Gold Antifade Mountant with DAPI	Life Technologies	Cat# P36931
Crystal violet	Acros organics	Cat# 229641000
Agar	Fisher	Cat# BP160
Fetal Bovine Serum, charcoal stripped	Gibco	Cat# 12-676-029
Matrigel	Corning	Cat# 354230
Dynabeads™ Protein G	Invitrogen	Cat# 10004D
Dynabeads™ Protein A	Invitrogen	Cat# 10002D
XeneLight D-Luciferin Potassium Salt	PerkinElmer	Cat# 122799
Critical commercial assays		
RNeasy Mini kit	Qiagen	Cat# 74106
Super-Script III First-Strand Synthesis Super-Mix Kit	Thermo Scientific	Cat# 18080400
PowerUp SYBR Green Master Mix	Applied Biosystems	Cat# A25742
Lipofectamine 3000 Transfection Reagent	Invitrogen	Cat# L3000015
Lipofectamine™ RNAiMAX Transfection Reagent	Invitrogen	Cat# 13778150
Dual-Glo® Luciferase Assay System	Promega	Cat# E2920
TruSeq RNA Sample Prep Kit ver.2	Illumina	Cat# IP-202-1012
Gateway LR Clonase II enzyme mix	ThermoFisher	Cat# 11791020
Gateway BP Clonase II enzyme mix	ThermoFisher	Cat# 11789100
Deposited data		
Phosphoproteomics data	This paper	ProteomeXchange: PXD028271
ChIP-sequencing data	This paper	GEO: GSE214332
Transcriptome of prostate cancer patient samples	Grasso et al.[1]	GEO: GSE35988
Transcriptome of prostate cancer patient samples	Taylor et al.[2]	GEO: GSE21032
Transcriptome of prostate cancer patient samples	Lapointe et al.[3]	GEO: GSE6469
Transcriptome profiling of siARVs in 22Rv1 cells	He et al.[75]	GEO: GSE80741
Transcriptome profiling of ARVs in CWR22Rv1 cells	Kounatidou et al.[76]	GEO: GSE126306
Transcriptome of prostate cancer patient samples	Abida et al.[6]	https://github.com/cBioPortal/datahub/tree/master/public/prad_su2c_2019; dbGap: phs000915.v1.p1.
Experimental models: Cell lines		
DU145	ATCC	Cat# HTB-81
22Rv1	ATCC	Cat# CRL-2505
VCaP	ATCC	Cat# CRL-2876
LNCaP	ATCC	Cat# CRL-1740
C4-2	ATCC	Cat# CRL-3314
HEK293	ATCC	Cat# CRL-1573
RWPE-1	ATCC	Cat# CRL-11609
E006AA	Millipore	Cat# SCC102
GP2-293	Clontech	Cat# 631458
DU145-DR	Rodriguez-Bravo et al.[56,57]	N/A
22Rv1-DR	Rodriguez-Bravo et al.[56,57]	N/A
VCaP-DR	This study	N/A

(Continued on next page)

Continued

REAGENT or RESOURCE	SOURCE	IDENTIFIER
DU145 histone H2B-mCherry	This study	N/A
DU145-DR histone H2B-mCherry	This study	N/A
22Rv1 histone H2B-mCherry	This study	N/A
22Rv1-DR histone H2B-mCherry	This study	N/A
VCaP histone H2B-mCherry	This study	N/A
VCaP-DR histone H2B-mCherry	This study	N/A
22Rv1 Dox inducible FLAP empty vector (pInducer20 EV)	This study	N/A
22Rv1 Dox inducible FLAP-MASTL siResistant (pInducer20-FLAP-MASTL siR))	This study	N/A
DU145 Dox inducible FLAP empty vector (pInducer20 EV)	This study	N/A
DU145 Dox inducible FLAP-MASTL siResistant (pInducer20-FLAP-MASTL siR)	This study	N/A
22Rv1-DR Dox inducible FLAP empty vector (pInducer20 EV)	This study	N/A
22Rv1-DR Dox inducible FLAP-MASTL siResistant (pInducer20-FLAP-MASTL-siR)	This study	N/A
22Rv1 FLAP empty vector (pQCXIN-FLAP EV)	This study	N/A
22Rv1 FLAP-MASTL siResistant (pQCXIN-FLAP-MASTL siR)	This study	N/A
DU145 FLAP empty vector (pQCXIN-FLAP EV)	This study	N/A
DU145 FLAP-MASTL siResistant (pQCXIN-FLAP-MASTL siR)	This study	N/A
PDX#1	Vidal et al.[55,82]	N/A
PDX#2	Vidal et al.[55,82]	N/A
PDX#3	This study	N/A
PDX#4	This study	N/A
Experimental models: Organisms/strains		
NOD.Cg-Prkdc[scid] IL2rg[tm1Wjl] (NSG) mice	Jackson mice	Cat# 005557
Oligonucleotides		
See Table S6		N/A
Recombinant DNA		
lentiCRISPR v2	Addgene	Cat# 52961
lentiCRISPR v2 - sghMASTL	Álvarez-Fernández et al.[62]	N/A
rtTA3-IRES-EcoR-Puro (RIEP2)	Rodriguez-Bravo et al.[56]	N/A
TRIN-E vector	Rodriguez-Bravo et al.[56]	N/A
pDONR221	ThermoFisher	Cat# 12536017
pInducer20	Stephen Elledge	Addgene 44,012
pInducer20-FLAP-(3xFlag-GFP)-MASTL siRNA resistant	This paper	N/A
pInducer20-FLAP-(3xFlag-GFP) empty vector	This paper	N/A
pQCXIN	Clontech	Cat# 631514
pQCXIN-FLAP-DEST-MASTL WT siRNA resistant	This paper	N/A
pQCXIN-FLAP-DEST-MASTL KD, G44S siRNA resistant	This paper	N/A
pQCXIN-FLAP-DEST empty vector	Rodriguez-Bravo et al.[24,56]	N/A
pQCXIB-H2B-mCherry	Rodriguez-Bravo et al.[24,56]	N/A

(Continued on next page)

Continued

REAGENT or RESOURCE	SOURCE	IDENTIFIER
pGL4.10 (luc2) reporter vector	Promega	Cat# E6651
pGL4.10 MASTL promoter wt	This paper	N/A
pGL4.10 MASTL promoter AR-V7 mutant	This paper	N/A
pRL-Renilla Luciferase Control Reporter Vector	Promega	Cat# E2231
pcDNA 3.1-AR-WT (AR-FL)	Hu et al.[68]	N/A
pcDNA 3.1-AR-V7	Hu et al.[68]	N/A
pVSV-G	Clontech	Cat# PT3343-5
psPAX2	Didier Trono	Addgene Cat#12260
Software and algorithms		
GraphPad	GraphPad	N/A
Fiji	NIH	https://imagej.nih.gov
Snapgene		https://www.snapgene.com/
SoftWoRx	GE Healthcare/Cytiva	N/A
MaxQuant	Cox et al.[108]	https://www.maxquant.org
g:Profiler	Reimand et al.[59]	https://biit.cs.ut.ee/gprofiler/gost
edgeR	Robinson et al.[109]	https://bioconductor.org/packages/release/bioc/html/edgeR.html
gsva	Hänzelmann et al.[110]	https://bioconductor.org/packages/release/bioc/html/GSVA.html
Living Image software v.4.2	PerkinElmer	http://www.perkinelmer.com

RESOURCE AVAILABILITY

Lead contact
Further information and requests for reagents should be directed to and will be fulfilled by the Lead Contact, Veronica Rodriguez-Bravo (RodriguezBravo.Veronica@mayo.edu).

Materials availability
Unique materials and reagents generated in this study will be made available upon request from the Lead contact and following Mayo Clinic reagent sharing policy.

Data and code availability
Data: mass spectrometric data are publicly available as of the date of publication via ProteomeXchange with identifier PXD028271. AR-V7 ChIP-Seq data generated by this study has been deposited in the Gene Expression Omnibus (GEO) with number GSE214332 and will be publicly available as of the date of publication. All other publicly available prostate cancer patient data used in this study were obtained from NCBI Gene Expression Omnibus databases GSE35988 (Grasso),[1] GSE21032 (Taylor)[2] and GSE6469 (Lapointe).[3] The CIN25 and CIN70 gene signatures were obtained from literature (Birkbak; Carter).[4,5] Transcriptomic data of AR variant-depleted (siRNA or CRISPR) prostate cancer cells were obtained from GEO datasets GSE80741 and GSE126306. RNA-seq data, including AR-V7 isoform was obtained from US2C/PCF Dream Team[6] and TCGA PRAD datasets using the cBioPortal Cancer Genomics portal. FGA scores are available on cBioPortal (https://www.cbioportal.org/) and can be downloaded in.txt file format. Bioinformatic analysis was performed using R version 4.0.3 (2020-10-10) and packages for R/Bioconductor detailed in the Reporting Summary accompanying this publication.
2. Code: no new code was created for analysis. Source data are provided with this paper. All software tools used in this study are listed in the STAR Methods description.
3. General Statement: any additional information required to re-analysis the data reported in this work paper is available from the lead contact upon request.

EXPERIMENTAL MODEL AND SUBJECT DETAILS

Cell lines and prostate cancer xenografts models
Prostate cancer cells 22Rv1, DU145, VCaP, LNCaP, C4-2, and HEK293 cells were obtained and authenticated (SRT, Short Tandem Repeat) from ATCC. E006AA primary prostate cancer cells were obtained, SRT authenticated, from Millipore. GP2-293 cells were a

gift from the Lujambio lab. Castration- and chemotherapy-resistant PCa cells (DU145-DR, 22Rv1-DR and VCaP-DR) were generated as previously described.[54,56,57] Briefly, Docetaxel-Resistant cells, were generated by culturing cells with vehicle (DMSO) or docetaxel in a dose-escalation manner using 72 h exposures. After several passages docetaxel resistant phenotype of the pooled populations was confirmed by colony formation assays and q-PCR of selected genes. PCa cells were maintained in RPMI media (Gibco) (22Rv1, DU145, LNCaP, C4-2), DMEM (ATCC) (VCaP) and DMEM (Gibco) (HEK293 and GP2-293), supplemented with 10% FBS (Gemini) and 1% penicillin/streptomycin (Gibco). To assess cell growth of cells under steroid-depleted conditions, cells were cultured with phenol red-free media supplemented with 10% charcoal dextran-treated FBS (Gibco). All cells were grown at 37°C in a humidified atmosphere with 5% CO_2. Advanced aggressive PCa xenograft models (PDX#1, PDX#2, PDX#3 and PDX#4) generated from circulating tumor cells from PCa patients as described previously[55,56,82] were used to test the *in vivo* activity of GKI-1 alone and in combination with standard-of-care therapy.

Human prostate cancer tissue samples

De-identified human formalin fixed paraffin embedded primary (n = 25) and advanced metastatic PCa tissue samples (n = 20) treated (n = 10) or not (n = 10) with taxane therapy were collected from the Mount Sinai GU Biorepository (IRB#11–01565) under Institutional Review Board approved protocol and provided by the NCI Cooperative Human Tissue Network (CHTN) as they became available (no sample size estimation was possible). All tissue sections were reviewed by a pathologist to confirm PCa origin. Informed consent from participants was obtained in both cases. No information was provided about health/immune status, previous procedures, or allocation of experimental groups.

Animal experimental models, husbandry and surgical castration

Mouse experiments were performed in accordance with NIH guidelines, approved and overseen by the Institutional Animal Care and Use Committee (IACUC) at Mayo Clinic and Thomas Jefferson University. Animal housing and husbandry was performed in accordance with institutional guidelines under the approved protocols. All experiments were performed with NOD.Cg-Prkdc[scid] IL2rg[tm1Wjl] (NSG) mice (Jackson Laboratories) using castrated male animals unless otherwise specified. For intracardiac injections, 3–4 weeks old mice were used. For the rest of the experiments 6–7 weeks old mice were used. For castration, anesthetized and surgically prepared animals were placed in dorsal recumbency. Both testes were then pushed down into the scrotal sacs by pressuring the abdomen. A 1cm incision was made in the scrotum to expose the tunica. The tunica was pierced, the testes were pushed out one at a time and then raised to expose the underlying blood vessels. The vas deferens with the prominent blood vessels running along them were located using a forceps and the testis were dissected away from the fat and removed. The vas deferens and ducts were then replaced back into the tunica, and skin incisions were closed with stainless steel wound closures and removed after 10 days.

METHOD DETAILS

Focused loss-of-function genetic screen of clinically up-regulated cell division kinases

Two independent custom siRNAs against eleven clinically up-regulated mitotic kinases were obtained from Life Technologies (Silencer Select siRNA) or from Dharmacon/Horizon. PCa cell parental line models and DR derivatives (DU145-DR, 22Rv1-DR and VCaP-DR) were used. Efficacy of depletion for each kinase (mRNA decrease >80%) was evaluated by quantitative RT-PCR (see STAR Methods details below) assessed starting at 48h post-transfection. DU145/DR and 22Rv1/DR cells were electroporated using the Neon Transfection System (Thermo Fisher) following the same manufacturer instructions. VCaP/DR cells were plated in 6-well plates and transfected with specific siRNAs or mock transfected using Lipofectamine RNAIMAX (Life Technologies). Functional evaluation to consider a gene a "hit" affecting therapy-resistant PCa cells (CRPC-DR) was reduced survival measured by colony formation assays.

RNA extraction and quantitative RT-PCR

RNA was isolated using the RNeasy Mini kit (Qiagen) in accordance with manufacturer's instructions. cDNA was synthesized from equivalent concentrations of total RNA using the Super-Script III First-Strand Synthesis Super-Mix Kit (Invitrogen) in accordance with manufacturer's instructions and the SimpliAmp thermal cycler systems (Applied Biosystems). Amplification was performed using a QuantStudio 3 Real-Time PCR System (Applied Biosystems). Cycle threshold values were determined and normalized to the loading control for each experiment. Fold changes for experimental groups relative to respective controls were calculated using MX Pro software (Agilent Technologies).

Genetic editing by CRISPR/Cas9 system

Genome editing of *MASTL* was performed with the CRISPR/Cas9 system as reported previously.[62] Briefly, sgRNAs targeting *MASTL* were designed according to available algorithms (http://crispr.mit.edu/) and subcloned into lentiCRISPRv2 vector (Addgene 52,961) following a rigorous method to exclude potential off-target effects of sgRNA *MASTL*. PCa cells were transduced with viral particles of empty vector or sgRNA *MASTL*#2 (TCCTTCTTGCTTCCCGCGGTGGG). Cells were then processed for subsequent analyses.

Inducible shRNAs

For inducible shRNA mediated knockdown of MASTL, two clones, shRNA#1 MASTL.1079 and shRNA#2 MASTL.1289 as well as a non-targeting Renilla control were selected following the screen of a custom library. Predictions of shRNA were obtained using "sensor rules" to enrich for predictions harboring sequence features associated with effective shRNAmir processing and potent knockdown.[111] DU145-DR and 22Rv1-DR cells were infected with a lentivirus containing a reverse tetracycline-controlled *trans*-activator 3 (rtTA3)-IRES-EcoR-Puro (RIEP2) and selected with puromycin (2 μg/mL) to generate stable cells. Subsequently, cells were infected with retroviruses containing a TRIN-E vector with the control or MASTL-targeting shRNAs and selected with neomycin (0.5 mg/mL). MASTL depletion efficiency was evaluated by immunoblotting 72 h after the addition of doxycycline (1 μg/mL) to culture media. RIEP2 and TRIN-E vectors were a generous gift from Dr. Amaia Lujambio (Mount Sinai School of Medicine, NY, USA).

Plasmids and viral transduction

FLAP (3xFlag-GFP)-MASTL cDNA carrying silent mutations to make it MASTL resistant to MASTL siRNAs (siR) used in this study was cloned into the entry vector pDONR221 (ThermoFisher) and moved into the doxycycline inducible lentiviral destination vector pInducer20 (gift from Stephen Elledge, Addgene plasmid #44012) via gateway cloning. The resulting constructs were co-transfected with a vesicular stomatitis virus glycoprotein envelope expression (pVSV-G) and PAX2 (gift from Didier Trono, Addgene plasmid #12260) plasmids into viral production cells GP2-293 cells (gift from Lujambio lab) following standard protocols previously described.[56] Infectious supernatants were filtered, diluted 1:1 with complete medium containing 20 μg/mL polybrene, and applied to target cells for 24 h. Selection with neomycin (0.4 mg/mL) was initiated 48 h later and stable populations validated and used for subsequent experiments. Similar steps were followed to clone FLAP-MASTL-siR into a pQCXIN-FLAP vector[24] and to generate viral particles to infect target cells. Finally, pQCXIB histone H2B-mCherry retroviral vector[24] was co-transfected with pVSV-G into GP2-293 cells and virus particles collected as above to infect target cells followed by selection with Blasticidin (10 μg/mL).

Colony formation assays

Clonogenic assays were performed by plating 10^3 cells in 6-well culture dishes after siRNA. For drug treatment analysis cells were plated and after 24 h treated with vehicle controls or with indicated drugs for 72 h (docetaxel) or continued exposure (GKI-1). After 10–14 days cell culture plates were washed with PBS, stained with a 2% crystal violet 10% formalin solution and formed colonies counted macroscopically.

Population doubling assays

Proliferation capacity of PCa cells were performed by plating 10^4 cells in 35mm culture dishes and counting the number of cells at indicated time points using an automated cell counter (Countess II Life Technologies).

Quantitative proteomics (SILAC) methods

Amino acid labeling in cell culture

Parental 22Rv1 and syngenic chemoresistant 22Rv1-DR cells were adapted to grow in SILAC RPMI-1640 media deficient in lysine and arginine (Thermo 88,365) supplemented with antibiotics (Pen/Strep), 10% dialyzed fetal bovine serum (Gemini) and normal amino acids "Light Amino Acid Media, Arg⁰,Lys⁰" (175 μM L-arginine (Arg0) plus 250 μM L-lysine (Lys0)), or with the same concentrations of stable isotope-labeled amino acids to make "Heavy Amino Acid Media, Arg,^{13} Lys^2" (L-arginine-^{6}C$_6$, ^{15}N$_4$ hydrochloride (Arg10) and L-lysine-^{6}C$_6$, ^{15}N$_2$ hydrochloride (Lys8), Cambridge Isotope Labs) as described before.[58] After six cell doublings and confirmation via mass spectrometry that heavy amino acids incorporation was equal or above 98% we proceeded with the experiment. Cells growing in 15 cm dishes at 70% confluence were accumulate din mitosis by treatment with 200 ng/ml nocodazole for 14 h, cells arrested in prometaphase collected by shake-off as previously described[24] and snap-frozen until sample preparation for mass spectrometry. Labeling scheme included three forward biological replicates (DR cells heavy/parental cells light) and three reverse replicates (DR cells light label/parental cells heavy).

Sample preparation and mass spectrometry

Samples were prepared for lysis in denaturing buffer (8 M urea, 50 mM Tris-HCl pH 8.2, 75 mM NaCl plus protease and phosphatase inhibitors (Roche) and processed as previously described.[112] Briefly, pellets were lysed in followed by incubation 15min on ice, sonicated and spun down for 35 min at 10,000g 4C. Cell extracts were quantified and light and heavy samples mixed 1:1. After pooling the SILAC-labeled cell lysates, samples were processed for digestion and phosphopeptide enrichment and analyzed by mass spectrometry following standard protocols.[112] The purified peptides were diluted to 0.1% formic acid and fraction/section was analyzed separately by microcapillary liquid chromatography with tandem mass spectrometry using the NanoAcquity (Waters) with a 100-μm-inner-diameter × 10-cm-length C18 column (1.7 μm BEH130, Waters) configured with a 180-μm × 2-cm trap column coupled to a Q-Exactive Plus mass spectrometer (Thermo Fisher Scientific). Key parameters for the mass spectrometer were: AGC 3 E6, resolution 70,000, 380–1800 *m/z*, top 10 method.

Data processing and statistical analysis

All MS/MS data was processed with the MaxQuant software (Max Planck Institute of Biochemistry, Martinsried, Germany; version 1.5.3.30).[108] The default was used for first search tolerance and main search tolerance: 20 and 6 ppm, respectively. Labels were set to Arg10 and Lys8. MaxQuant was set up to search the reference human proteome database downloaded from Uniprot on

Sept 6, 2016. Maxquant performed the search assuming trypsin digestion with up to two missed cleavages. Peptide, site, and protein FDR were all set to 1% with a minimum of 1 peptide needed for identification but two peptides needed to calculate a protein level ratio. The following modifications were used as variable modifications for identifications and included for protein quantification: oxidation of methionine, acetylation of the protein N-terminus, phosphorylation of serine, threonine and tyrosine residues, and carbamidomethyl on cysteine. Specific phosphosites were assigned by the MaxQuant PTM score algorithm[113,114] resulting on identification of around 13,000 phosphopeptides. Phosphopeptides measured in all six biological replicates were log2-transformed. "Reverse" and "Potential contamination" are filtered out, then phosphopeptides are filtered with all ratios present in 6 replicates, resulting in 1,162 peptides, plotted and statistically analyzed via ANOVA. Fold changes (Log2FC) $\geq$ 1.5 and Benjamini-Horchberg FDR <0.05 in 22Rv1-DR cells vs. parental cells were rated as significant. P-value was adjusted for multiple testing using Benjamini Horchberg method. Phophoproteins increased in 22Rv1-DR cells in at least 3 replicates were query for functional enrichment analysis using gProfiler[59] to determine significantly enriched Gene Ontology Biological Processes. P-value was computed by Fisher's test and corrected with Benjamini-Hochberg FDR. The mass spectrometry data have been deposited to the ProteomeXchange Consortium via the PRIDE[115] partner repository with the dataset identifier PXD028271.

Bioinformatic analysis

Transcriptome profiling of publicly available prostate cancer patients were obtained from NCBI Gene Expression Omnibus databases GSE35988,[1] GSE21032[2] and GSE6469.[3] Bioinformatics data analysis was performed using R software version 4.0.3. Data analysis compared gene expression changes between primary (n = 59) and warm autopsy (n = 35) lethal prostate cancer patients from Grasso et al. dataset, primary (n = 127) and metastatic (n = 9) patients from the Taylor et al. dataset and primary (n = 62) and metastatic (n = 9) from Lapointe et al. Differential expression was assessed between sample groups using the two-sided Welch's t-test, and the false discovery rate (FDR) was estimated using the Benjamini-Hochberg Procedure. Fraction of genome altered (FGA) estimates of prostate tumors, representing chromosome heterogeneity affected by copy number gains or losses as previously reported,[19] were downloaded from cBioPortal for available datasets including Taylor, TCGA PRAD and the metastatic US2C/PCF Dream Team studies.[2,6,16,63] The CIN25 and CIN70 gene signatures were obtained from literature.[4,5] The GSVA package in R/Bioconductor was used to estimate single-sample gene set enrichment scores for the CIN25 and CIN70 gene lists in each patient sample.[110] Pearson correlation coefficients between FGA and CIN scores and known human transcription factors[116] were computed in these datasets to identify potential regulatory transcriptional networks enriched with chromosomal instability in advanced prostate cancer tumors. A consensus correlation coefficient and p value were estimated by performing correlation meta-analysis across all datasets using the meta package in R.[117] Each study was weighted using the inverse variance method, with a random effects model using the DerSimonian-Laird method, and statistics were based on the Fisher z-transform for correlation. Mitotic kinase genes were evaluated for differential expression in two AR-V knockdown experiments (siRNA and CRISPR), obtained from GEO datasets GSE80741 and GSE126306.[75,76] Differential expression fold-changes, p values, and FDR estimates were generated from transcript counts using the edgeR package in R/Bioconductor.[109] Normalized Trimmed Mean of M-values (TMM) from edgeR were used to visualize changes in the knockdown groups. RNA-seq data, including AR-V7 isoform was obtained for TCGA PRAD and SU2C/PCF Dream Team datasets using the cBioPortal.[6,16,63,118] These data were used to estimate both Pearson and Spearman correlations between AR-V7, MASTL, FGA score and CIN gene signature mRNA expression. Correlations were estimated in the subset of TCGA PRAD RNA-seq samples containing transcriptomic data from PC tissue samples that had detectable levels of AR-V7 (n = 38) as previously described.[75] Similarly, Pearson and Spearman correlation analysis between MASTL and E2F7 mRNA expression were performed using TCGA PRAD,[63] GSE35988[1] and validated in a dataset containing only metastatic samples (SU2C).[6]

Cell synchronization, extract preparation and immunoblotting

Asynchronous or synchronized (mitotic) cell pellets obtained after arresting cells with nocodazole 200 ng/ml for 14h before shake off, were washed twice with PBS and snap-frozen in a dry ice-methanol bath. Whole cell extracts were prepared by resuspending cell pellets in buffer B (140 mM NaCl, 30 mM HEPES, pH 7.8, 5% glycerol, 10 mM sodium pyrophosphate, 5 mM sodium azide, 10 mM NaF, 10 mM PMSF, 0.3 mM sodium orthovanadate, 20 mM β-glycerophosphate, 1 mM DTT and 1× protease and phosphatase inhibitor cocktail (Roche) followed by nitrogen cavitation (1250 psi, 45 min; Parr Instruments) and centrifugation at 20,000g for 15 min at 4C as previously described by us.[24] Final samples were resuspended in 1× Laemmli sample buffer, boiled for 5 min and SDS-PAGE resolved proteins were transferred to nitrocellulose membranes and incubated with primary antibodies and anti-rabbit and anti-mouse horseradish peroxidase (HRP) conjugated secondary antibodies (Cytiva NA931 and NA935). Chemoluminescence was measured after incubation with ECL detection reagent (RPN2236) using the Imager Amersham 600 system (Cytiva) and quantified using Fiji (ImageJ/NIH).

Immunofluorescence microscopy

For immunofluorescence microscopy cells were grown on glass coverslips, samples were simultaneously fixed and permeabilized in 4% PFA, 20 mM Pipes, pH 6.8, 10 mM EGTA, 1 mM MgCl2 and 0.2% Triton for 10 min at room temperature. After blocking in 6% BSA for 1 h coverslips were incubated in primary antibody for 2 h at room temperature, followed by PBS washes and incubation with Alexa 488-, 568-, and 647-conjugated secondary antibodies. Cells were counterstained with DAPI prior to mounting in Prolong Gold (Invitrogen). Images were acquired on an Applied Precision DeltaVision Ultra microscope (Cytiva) with a 60 ×1.4NA oil objective

and deconvolved using Softworx. Maximum intensity projections of z-stacks (mitotic cells) or single optical sections (interphase cells) were analyzed in ImageJ. Quantitative image analysis was performed using Fiji. Anaphase chromosome missegregation and other mitotic errors were identified and scored using the DAPI and kinetochore (CREST) staining as reference.

Live-cell imaging
Cells stably expressing histone H2B-mCherry were grown on glass bottom multiwell plates for imaging (Cellvis). Widefield and phase-contrast images were acquired on an Applied Precision DeltaVision Ultra microscope equipped with 20× long working distance, a temperature-controlled stage enclosure with CO2 support, and processed with Softworx and ImageJ for scoring chromosome segregation errors (lagging chromatids and others) and mitotic timing scoring (time from nuclear envelope breakdown or NEBD to DNA decondensation). Higher resolution images of cell division were acquired in same microscope and conditions using a 60 ×1.4NA oil objective, deconvolved using Softworx and subjected to maximum z stack projections. Individual images were cropped and assembled into figures using Fiji/ImageJ and Photoshop (Adobe).

Immunohistochemistry
Immunohistochemistry (IHC) analyses were conducted on PCa formalin fixed paraffin embedded tissue sections from human samples and in cell line or lethal PCa (LPC) xenografts. Tissue sections (5μm) were deparaffinized and submitted for standard perox-idase-based immunohistochemistry procedures. Quantification of positive cells was determined by counting the number of tumor cells in 10 contiguous high-power fields in three different areas of each section and referred to the total number of counted cancer cells. MASTL, AR-V7 and E2F7 protein expression were analyzed in PCa formalin fixed paraffin embedded tissue samples. Samples were scored as MASTL, AR-V7 or E2F7 "low" when completely negative staining or when <5% PCa cells displayed nuclear staining and "high" when ≥5% of PC cells displayed nuclear staining in 4 contiguous high-power fields in three different areas of each section.

Evaluation of chromosome segregation errors in tumor tissue samples
PCa tissue specimens (25 primary tumors and 20 metastatic tumors) were stained with hematoxylin/eosin (H&E) and analyzed to score anaphases with chromosome missegregation events with a light microscope. Lagging chromosomes and chromatin bridges were scored as chromosome missegregation events and computed as proxies for total CIN. Percentage of anaphases with chromosome segregation errors was determined in 10 contiguous high-power fields in three different areas of each section.

Chemical treatments
The following chemicals were used in this study: MG132 (10 μM), nocodazole (200 ng/mL), GKI-1 (10 μM unless otherwise indicated), docetaxel at indicated concentrations. 100 μM Monastrol treatment for anaphase enrichment (5h treatment plus 45-min release after washout). Induction of transgene expression with doxycycline 1 μg/mL. Antibiotics for cell line selection included 0.5 mg/mL genet-icin, 10 μg/mL blasticidin or 2 μg/mL puromycin. For enrichment in mitotic populations cells were treated for 14h with nocodazole and mitotic cells separated by shake off as described before.[24] For *in vitro* testing of GKI-1 inhibition, cells were treated with nocodazole and MG132 combination to avoid potential premature mitotic exit.

Chromatin immunoprecipitation (ChIP)
Cells were cross-linked incubating with 1% formaldehyde solution 10 min at room temperature followed by glycine addition to stop crosslinking. Chromatin was obtained by lysing cross-linked cells with Lysis Buffer 1 (LB1) (50mM Hepes-KOH, 140mM NaCl, 1mM EDTA, 10% Glycerol, 0.5%NP-40/Igepal, 0.25% Triton X-100) then LB2 (10mM Tris-HCl pH8, 200mM NaCl, 1mM EDTA, 0.5mM EGTA). Each lysis buffer was followed by gentle rocking on ice for 10 min prior to centrifugation at 4C. Cell pellets were resuspended in LB3 (10mM Tris-HCl pH 8, 1mM EDTA, 0.5mM EGTA, 0.1% Na-Deoxycholate, 0.5% N-laurylsarcosine sodium salt) and sonicated using a Bioruptor Pico sonication device (Diagenode). Sonicated chromatin samples were incubated overnight at 4C with antibody-conjugated protein A magnetic beads (Dynabeads, Thermo Fisher) in Blocking Buffer (0.5% BSA in 1x PBS). DNA-protein-antibody beads were then washed, and eluted chromatin decross-linked by incubating beads at 65C overnight in Elution Buffer (1% SDS, 0.1M NaHCO3) followed by RNAse A (Thermo Scientific) and Proteinase K (New England BioLabs) treatments. DNA was immunoprecip-itated by phenol:chloroform:isoamyl alcohol (P:C:IA) and analyzed by qPCR using specific primers. For ChIP sequencing, AR-V7 ChIP with anti-AR-V7 specific Precision AG10008 (ChIP, 5ug per sample) samples were submitted to Thomas Jefferson University Genomics Core Facility for preparation of multiplexed libraries and deep sequencing using the Illumina NextSeq 500 platform producing 75bp SE reads according to the manufacturer's instructions. FoR ChIP-Seq data analysis, sequences were aligned to the reference genome, using Burrows Wheeler Alignment tool (BWA).[119] Duplicated reads were removed, and MACS2 used to call individual peaks using input as controls, at 5% FDR, with default parameters.[120]

Luciferase reporter assays
HEK 293 cells were seeded into 12- well plates at a density of 1.25×10^5 and allowed to attach overnight. Transfection mix was prepared by combining 300ng of either pGL4.10 luc-MASTL wild type (wt), pGL4.10 luc-MASTL AR-V7 mutant (mut), 30ng of pRL-Renilla, and 600ng of pcDNA3 AR-V7, pcDNA3 AR-FL or empty expression vector (pcDNA3). Luciferase activity was measured

with Dual-Luciferase-Assay kit (Promega) 48 h after transfection, mixing 50μL of lysate with 50μL of Luciferase Buffer Assay (Dual Glo, Promega) and analyzed in an automatic luminometer (Promega GloMax Luminometer). 50μL of Stop & Glo reagent was then added and Renilla luminescence measured after 10 min of incubation. Ratios of Firefly versus Renilla luciferase were calculated to determine promoter activity.

Tumor growth *in vivo*

For *in vivo* studies involving shRNAs against MASTL and GKI-1 treatments, subcutaneous xenografts were generated by implantation of 10^6 indicated PCa cells in a 1:1 mixture of culture medium RPMI (Gibco) and Matrigel (Corning) into the flanks of NSG mice. When subcutaneous tumors became palpable, mice were randomly assigned to treatment groups containing four animals. The vehicles for chemotherapy and GKI-1 were 10% DMSO in sterile 1xPBS. Tumor dimensions were monitored weekly using Vernier calipers. Tumor volume was calculated according to the formula $V = (a^2 \times b)/2$ where a and b are the minimal and maximal diameter in millimeters, respectively. In accordance with institutional guidelines, mice bearing subcutaneous xenografts greater than 500mm³ were sacrificed. Explanted tumors were weighed, formalin fixed, and embedded in paraffin for pathological analysis.

Mouse intracardiac injections *in vivo* bioluminescence imaging

Intracardiac injections were performed as previously described.[121] Briefly, the ventral thorax of 3–4 weeks old, castrated males was shaved prior anesthesia with an isoflurane vaporizer and nose cone. The thorax was sterilized with iodine and alcohol and a sterile marker was used to mark a location halfway between the sternal notch and the xyphoid process. 100μL from a 1×10^5 cell/ml suspension of PCa cells and PDX cells in sterile 1xPBS was drawn into a 30.5 gauge needle. The upright syringe was gently inserted through the mark and for each injection successful penetration into the left ventricle was confirmed visually by a pulse of bright red blood into the syringe. Following each experiment, a detailed necropsy was performed to grossly and histologically confirm disseminated tumor burden. Imaging was performed using an IVIS Spectrum (Xenogen) imager. Animals received luciferin at 200 mg/kg by intraperitoneal injection 5 min prior to imaging. Animals were then anesthetized using an isoflurane vaporizer and placed onto the warmed stage inside the camera box. At this stage animals received continuous exposure to 2% isoflurane. For quantification, rectangular regions of interest (ROIs) incorporating the entire animal were measured. The signal was measured in photons per second using Living Image software v.4.2 (Xenogen).

General toxicity monitoring

Body weights for every mouse were recorded every three days and fluctuations were computed by the percentage of current body weight relative to baseline. When animals showed signs of weight loss therapy was discontinued. In accordance with institutional guidelines all animals experiencing greater than 20% weight loss were sacrificed.

QUANTIFICATION AND STATISTICAL ANALYSIS

Data statistical analysis and graphical representation was carried out with Prism (GraphPad) and indicated in the figure legends and/or figure panels. All experiments were performed at least in three biological independent replicates and all data points visualized in the graphs. Data is expressed as mean ± SD (SD) from at least three independent experiments. For imaging quantification, a minimum of 100 cells were scored per condition analyzed in each experiment. Sample size and number of independent experiments (replicates) used for each figure is specified in the figure or figure legends. All experiments were reliably reproduced resulting in no experimental data being excluded from our analysis. Statistical analyses in cell lines quantifications were performed using Student's *t* test and ANOVA was used for proteomic analysis. P-value was computed by Fisher's test corrected with Benjamini-Hochberg FDR in Gene Ontology (GO) analysis of proteomic data with g:Profiler. For *in vivo* work planning of sample size was based on our previous experience and publications. To analyze correlations, we used Pearson and Spearman's correlation tests when the two variables were assessed as continuous, Student's *t* test when one variable was assessed as continuous and the other as qualitative and χ^2 test (Fisher exact test) when the two variables were qualitative. In pre-clinical survival studies analyses were performed using the Kaplan–Meier method and curves were compared by the log-rank test. More details on statistical analysis can be found in each article figure legend.

Supplemental information

Harnessing transcriptionally driven

chromosomal instability adaptation to target

therapy-refractory lethal prostate cancer

Brittiny Dhital, Sandra Santasusagna, Perumalraja Kirthika, Michael Xu, Peiyao Li, Marc Carceles-Cordon, Rajesh K. Soni, Zhuoning Li, Ronald C. Hendrickson, Matthew J. Schiewer, William K. Kelly, Cora N. Sternberg, Jun Luo, Amaia Lujambio, Carlos Cordon-Cardo, Monica Alvarez-Fernandez, Marcos Malumbres, Haojie Huang, Adam Ertel, Josep Domingo-Domenech, and Veronica Rodriguez-Bravo
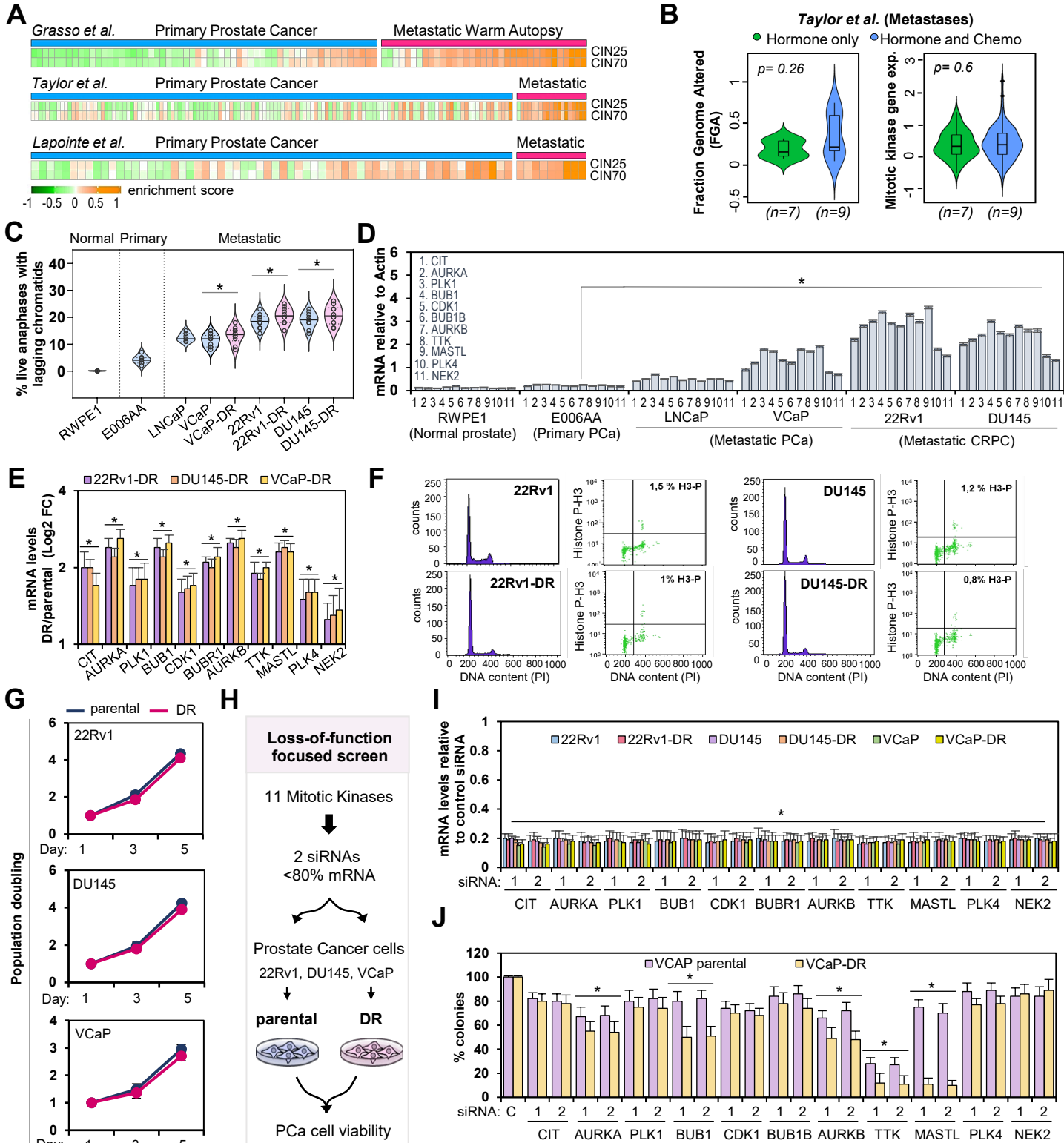
Figure S1. Chemotherapy resistant PCa cells recapitulate the highest CIN and mitotic kinase levels observed in patients without changes in proliferation rates. Related to Figure 1. (A) CIN enrichment in primary and metastatic tumors from 3 publicly available PCa patient datasets[7-9]. Orange=high, green=low. **(B)** FGA and mitotic kinase gene expression in hormone or hormone + chemotherapy treated metastases from a PCa dataset[8]. p-value, Wilcoxon's test. **(C)** Percentage of lagging chromosomes (live imaging) in indicated prostate cell lines. ∗p ≤ 0.05, determined by Wilcoxon's test. **(D)** mRNA expression levels of clinically upregulated mitotic kinases in prostate cells. **(E)** mRNA expression levels of same kinases comparing DR and parental PCa cells. **(F)** Representative DNA content and percentage of phosphorylated histone H3 (mitotic marker) by flow cytometry comparing parental and DR cells. **(G)** Population doubling analysis comparing parental and DR PCa cells. **(H)** Diagram of focused loss-of-function screen to assess viability in parental and DR PCa cells. **(I)** Mitotic kinase mRNA expression in parental and DR cells 72h after siRNAs. **(J)** Colony formation quantification in VCaP parental and DR PCa cells after control or mitotic kinases siRNA. Unless indicated, data represent the mean ± SD of at least 3 independent experiments. ∗p ≤ 0.05, determined by Student's t-test.

A
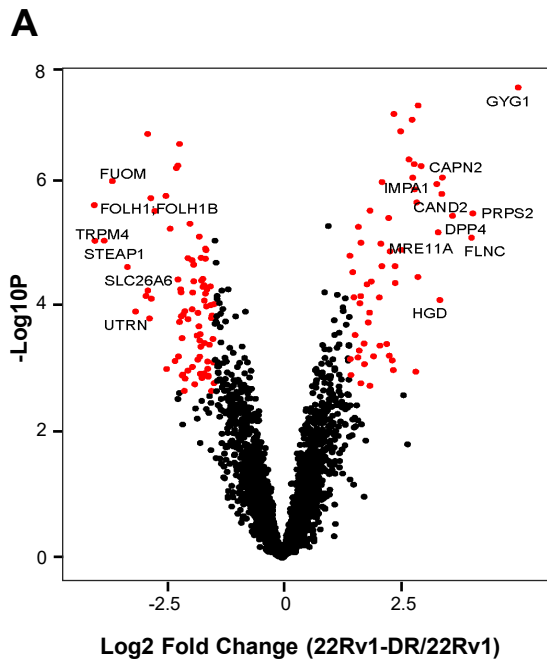
B

Top Mitotic peptides (DR/parental p≤0.05)

| Gene name	Protein name	Fold change
ESPL1	Separase	2.5
CCNB1	G2/mitotic-specific cyclin-B1	2
CDC27	Cell division cycle protein 27 homolog	1.8
KIF14	Kinesin-like protein KIF14	1.8
PLK1	Serine/threonine-protein kinase PLK1	1.7
CIT	Citron Rho-interacting kinase	1.75
KIF2C	Kinesin-like protein KIF2C;Kinesin-like protein	1.7
AURKB	Aurora kinase B	1.65
ASPM	Abnormal spindle-like microcephaly-associated protein	1.6
AURKA	Aurora kinase A	1.5
CENPF	Centromere protein F	1.5
MASTL	Serine/threonine-protein kinase greatwall	1.4
KIF22	Kinesin-like protein KIF22;Kinesin-like protein	1.4
CDC7	Cell division cycle 7-related protein kinase	1.4
BUB1B	Mitotic checkpoint serine/threonine-protein kinase BUB1 beta	1.38
PRC1	Protein regulator of cytokinesis 1	1.25
INCENP	Inner centromere protein	1.25
TPX2	Targeting protein for Xklp2	1.25
BIRC5	Baculoviral IAP repeat-containing protein 5/surviving	1.25
ANLN	Actin-binding protein anillin	1.2
CDC2	Cyclin-dependent kinase 1	1.2

C

D
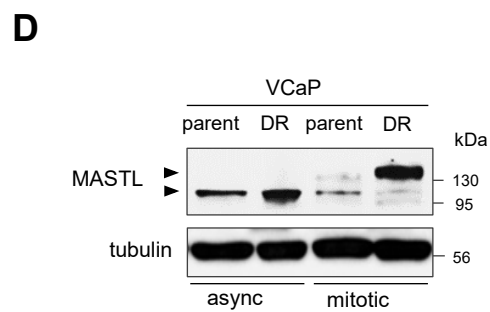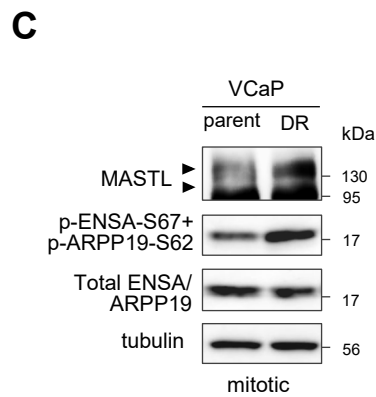
Figure S2. SILAC quantitative total proteome analysis identifies MASTL protein increase in therapy resistant lethal PCa cells. Related to Figure 2. (A) Volcano plot of top total proteome log2 fold changes comparing DR and parental cells. Red dots = significant changes by ANOVA analysis. **(B)** List of top upregulated cell division proteins in DR cells. **(C)** MASTL, total and phospho-ENSA/ARPP19 immunoblots of mitotic VCaP and syngenic VCaP-DR cells. **(D)** MASTL immunoblots of asynchronous or mitotic parental and DR VCAP cells. Arrows indicates changes in the mobility shift of MASTL protein in mitosis (unphosphorylated proteins migrate more quickly).
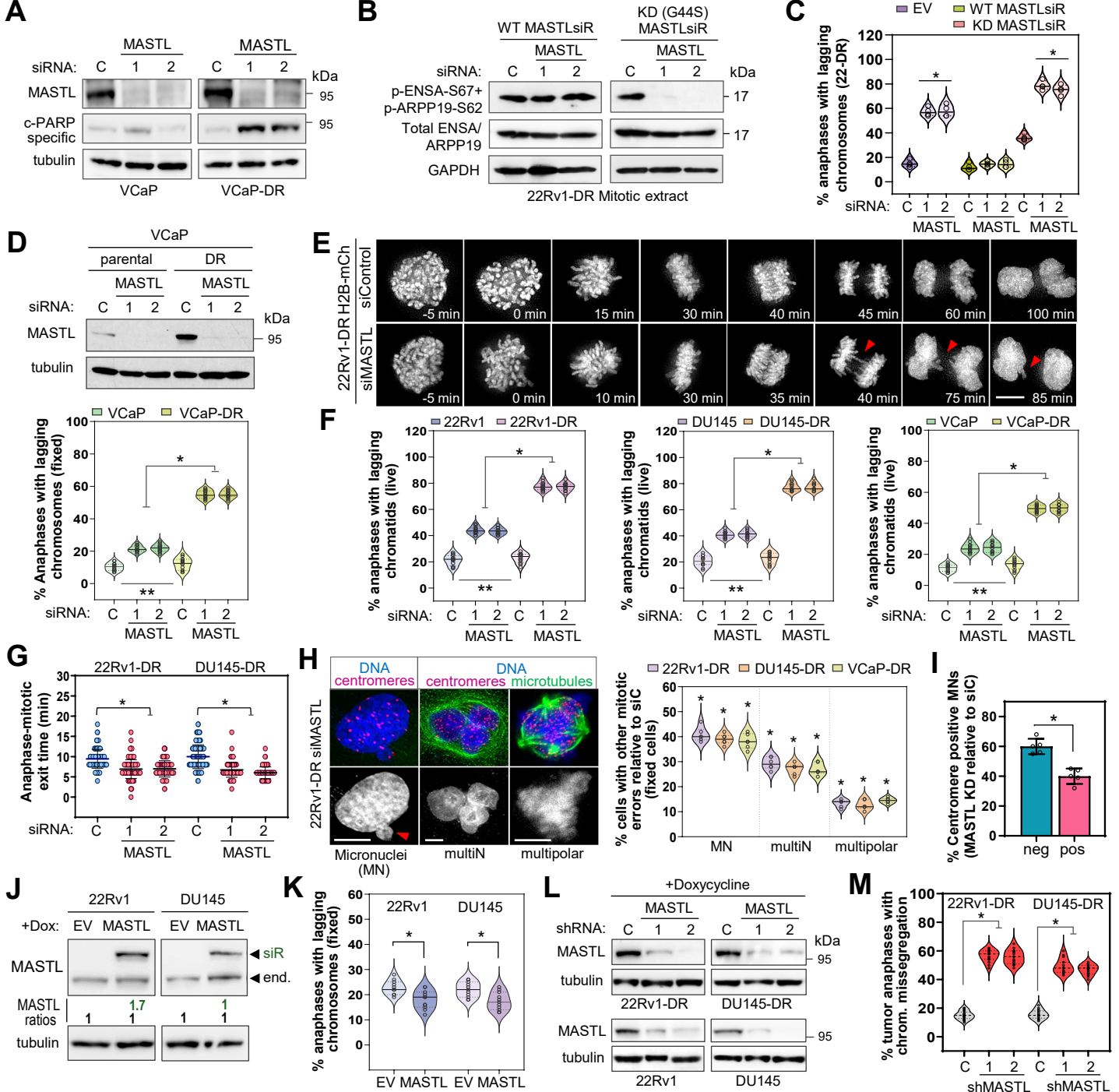
Figure S3. Chromosome segregation fidelity analysis in therapy-resistant MASTL-dependent PCa cells. Related to Figure 3.
(A) MASTL and cleaved PARP immunoblots in VCaP/DR cells 72 h after siRNAs. **(B)** Total and phospho-ENSA/ARPP19 immunoblots of mitotic cells doxycycline-induced to express wild type (WT) or kinase dead (G44S, KD) FLAP-MASTL siRNA resistant (siR) compared to empty vector (EV, FLAP) after siRNAs. **(C)** Percentage of lagging chromosomes in cells from **B**). **(D)** MASTL immunoblot and quantification of lagging chromosomes in cells 48h after siRNAs. *p ≤ 0.05, compares MASTL-depleted cells. **p ≤ 0.05, compares controls. Both determined by Wilcoxon's test. **(E)** DR cells' live imaging montage after siRNA. Arrow, lagging chromatids and micronuclei. **(F)** Quantification of lagging chromosomes in cells like in **E**). *p ≤ 0.05, compares MASTL-depleted cells. **p ≤ 0.05, compares controls. Both determined by Wilcoxon's test. **(G)** Anaphase-mitotic exit time in DR cells as in **E**). **(H)** Representative immunofluorescence and quantification of mitotic phenotypes after MASTL siRNA (multiN=multinucleated). Centromeres (CREST), microtubules (alpha-tubulin). Arrow, micronuclei. **(I)** Quantification of micronuclei with negative or positive centromeres from **H**). **(J)** MASTL immunoblots and quantifications relative to endogenous (end.) in parental cells after 72h of doxycycline to overexpress FLAP-MASTL siRNA resistant (siR) or empty vector. **(K)** Quantification of lagging chromosomes in cells from **J**). *p ≤ 0.05, determined by Wilcoxon's test. **(L)** MASTL immunoblots of parental and DR cells expressing control or MASTL shRNAs after 72h of doxycycline induction. **(M)** Percentage of chromosomes missegregation in DR xenografts expressing shControl (n=20) or two shMASTL (n=10 each/condition) treated with doxycycline for 4 days. Unless indicated, data represent the mean ± SD of at least 3 experiments. p-values, determined by Student's t-test. Minimum of 100 cells/condition scored. Bar 5 μm.
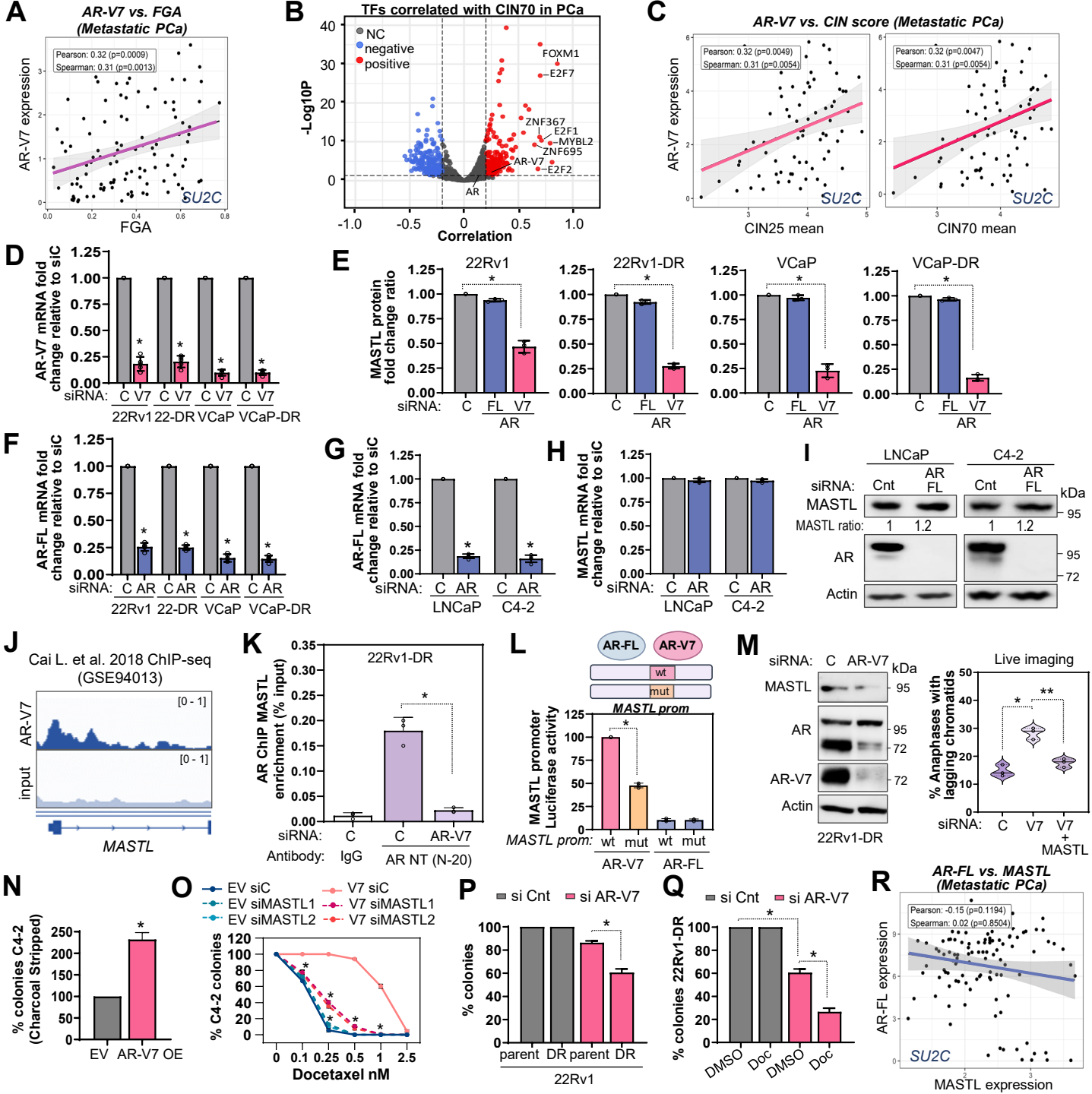
Figure S4. AR-V7 transcriptional regulation of *MASTL* restrains deleterious CIN in PCa cells. Related to Figure 4. (A) FGA/AR-V7 correlation (Pearson/Spearman) in the SU2C dataset[13]. **(B)** TFs/CIN70 correlation plot in patient datasets[8,13,63]. (NC) no correlated, p ≤ 0.05, by Fisher z-transform. **(C)** CIN 25/70 and AR-V7 correlation as in **A**). **(D)** AR-V7 mRNA levels after AR-V7 siRNA. **(E)** MASTL immunoblot quantification in control, AR-FL or AR-V7 siRNA. **(F)** AR-FL mRNA levels after AR-FL siRNA. **(G)** AR-FL mRNA levels in control/AR-FL siRNA in V7 negative cells. **(H)** MASTL mRNA levels from **G**). **(I)** MASTL and AR immunoblots from **G-H**). **(J)** AR-V7 22Rv1 ChIP-seq profile from a published study[77]at *MASTL* locus. **(K)** AR ChIP-qPCR occupancy at *MASTL* in 22Rv1-DR cells with antibody against both AR-FL and variants. **(L)** Luciferase assay (relative to vector control) in HEK293 cells co-transfected with a wild type (wt) or AR-V7 motif mutated (mut) MASTL promoter luciferase reporter, AR-V7 or AR-FL expressing vector and renilla control. **(M)** Immunoblots and quantification of lagging chromosomes in 22Rv1-DR. *p ≤ 0.05 compares control/AR-V7 siRNA. **p ≤ 0.05 compares AR-V7 siRNA and combined with MASTL overexpression. **(N)** Colony formation quantification of C4-2 cells overexpressing (OE) AR-V7 or control (EV). **(O)** Colony formation quantification of cells in **N**) after docetaxel and control/MASTL siRNA. **(P)** Colony formation quantification of 22Rv1 parental/DR cells after control/AR-V7 siRNA. **(Q)** Colony formation quantification of control/AR-V7 siRNA 22Rv1-DR cells after DMSO or 75nM docetaxel 72h.**(R)** AR-FL/MASTL correlation as in **A**). Unless indicated, data represent the mean ± SD of at least 3 experiments. *p ≤ 0.05, determined by Student's t-test.
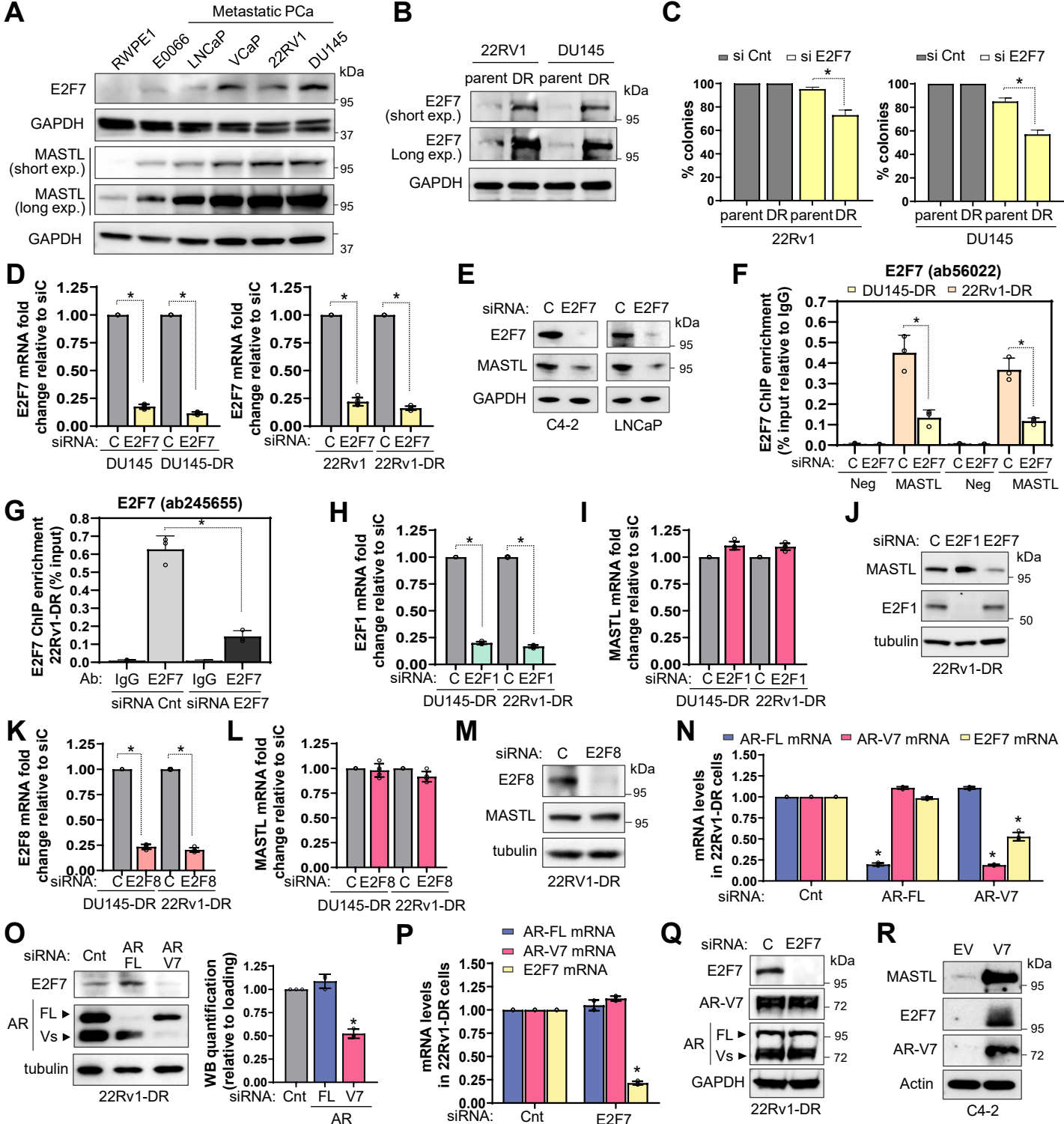
Figure S5. E2F7 is the main E2F regulating MASTL gene expression directly and through an AR-V7 crosstalk in PCa cells. Related to Figure 5. (A) E2F7 and MASTL immunoblots comparing normal prostate, primary and metastatic PCa cells. **(B)** E2F7 immunoblot comparing metastatic parental and DR cells. **(C)** Colony formation quantifications of parental and DR cells after control or E2F7 siRNA. **(D)** E2F7 mRNA levels from **C**). **(E)** E2F7 and MASTL immunoblot in AR-V7 negative cells after control or E2F7 siRNA depletions. **(F)** E2F7 ChIP-qPCR validation at *MASTL* promoter in DR cells. Flanking control region (Neg). **(G)** E2F7 ChIP-qPCR validation using an independent antibody (ab245655) as in **F**). **(H)** E2F1 mRNA levels 48h after control or E2F1 siRNA in DR cells. **(I)** MASTL mRNA levels in cells from **H**). **(J)** MASTL and E2F1 immunoblots in cells from **H-I**). **(K)** E2F8 mRNA levels 48h after control or E2F8 siRNA in DR cells. **(L)** MASTL mRNA levels in cells from **K**). **(M)** E2F8 and MASTL immunoblots in cells from **K-L**). **(N)** AR-V7, AR-FL and E2F7 mRNA levels 48h after control, AR-FL or AR-V7 siRNA in 22Rv1-DR cells. **(O)** Representative MASTL, E2F7 and AR immunoblots and quantifications from cells in (**N**). **(P)** AR-V7, AR-FL and E2F7 mRNA levels 48h after control or E2F7 siRNA in 22Rv1-DR cells. **(Q)** E2F7, AR-V7 and pan AR immunoblot in cells from (**P**). **(R)** MASTL, AR-V7 and E2F7 immunoblots in control (empty vector, EV) and AR-V7 overexpressing C4-2 cells. Unless indicated, data represent the mean ± SD of at least 3 experiments. *p ≤ 0.05, determined by Student's t-test.
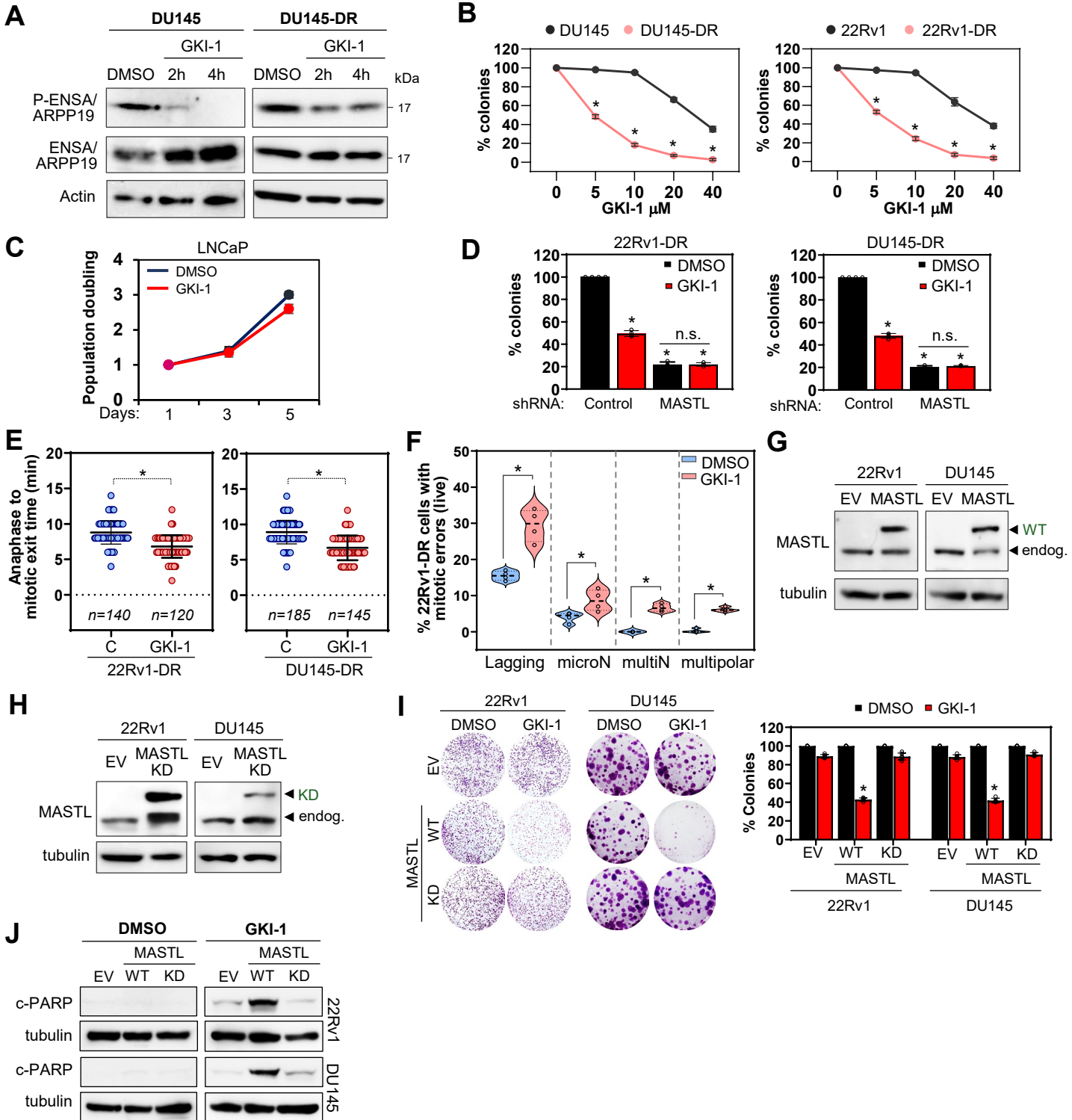
Figure S6. GKI-1 treatment phenocopies MASTL genetic depletion deleterious CIN phenotypes in PCa cells. Related to Figure 6. (A) MASTL, total and phospho-ENSA/ARPP19 immunoblots in mitotic parental and DR cells treated with GKI-1 for 2 or 4h. **(B)** Colony formation and quantifications of parental/DR cells treated with increasing concentrations of GKI-1. **(C)** Cell population doubling of LNCaP cells treated with vehicle (DMSO) or GKI-1. **(D)** Colony formation quantification of cells after control or shRNA MASTL treated with DMSO or GKI-1. Not significantly (n.s.). **(E)** Anaphase-mitotic exit time quantification via live imaging of histone H2B-mCherry DR cells treated with vehicle (DMSO) or GKI-1. **(F)** Quantification of mitotic phenotypes after vehicle (DMSO) or GKI-1 in 22Rv1-DR cells. **(G)** MASTL immunoblots in parental cells expressing wild type FLAP-MASTL (WT) or empty vector (FLAP, EV). **(H)** MASTL immunoblots in parental PCa cells expressing kinase dead FLAP-MASTL (KD) or empty vector (FLAP, EV). **(I)** Colony formation and quantifications in parental cells expressing wild type (WT), kinase dead MASTL (KD) or empty vector (EV), treated with GKI-1 (5 μM). **(J)** Immunoblots of cleaved PARP after 72h in cells from **I**). Unless indicated, GKI-1 used at 10μM. Minimum of 100 cells scored. Data represent the mean ± SD of at least 3 experiments. *p ≤ 0.05, determined by Student's t-test. Endogenous MASTL (endog.).

A

22Rv1   22Rv1-DR

T1 T2 T3 T4   T1 T2 T3 T4   kDa

MASTL   — 95

GAPDH

DU145   DU145-DR

T1 T2 T3 T4   T1 T2 T3 T4   kDa

MASTL   — 95

GAPDH

B

22Rv1   22Rv1-DR

veh.   GKI-1   veh.   GKI-1

Tumor weight (gr) — veh / GKI-1

22Rv1   DU145   22-DR*   DU-DR*

C

% weight vs Days (1, 4, 7, 10, 13, 16, 19, 22, 25, 28)

vehicle / GKI-1

D

% tumor anaphases with chromosome missegregation

veh GKI   veh GKI   veh GKI   veh GKI

22Rv1   DU145   22-DR   DU-DR

E

Sample	Previous Anti-androgen therapy	Previous Chemotherapy
PDX1 (AR-FL-, AR-V7-, E2F7 low)	ADT, Enzalutamide, Abiraterone	Docetaxel
PDX2 (AR-FL+, AR-V7+, E2F7 high)	ADT, Enzalutamide, Abiraterone	Docetaxel Cabazitaxel
PDX3 (AR-FL+, AR-V7-, E2F7 low)	ADT	none
PDX4 (AR-FL+, AR-V7+, E2F7 high)	ADT	Docetaxel

F

veh.   GKI-1   veh.   GKI-1   veh.   GKI-1   veh.   GKI-1

T1 T2   T1 T2   T1 T2   T1 T2   T1 T2   T1 T2   T1 T2   T1 T2   kDa

c-PARP   — 95
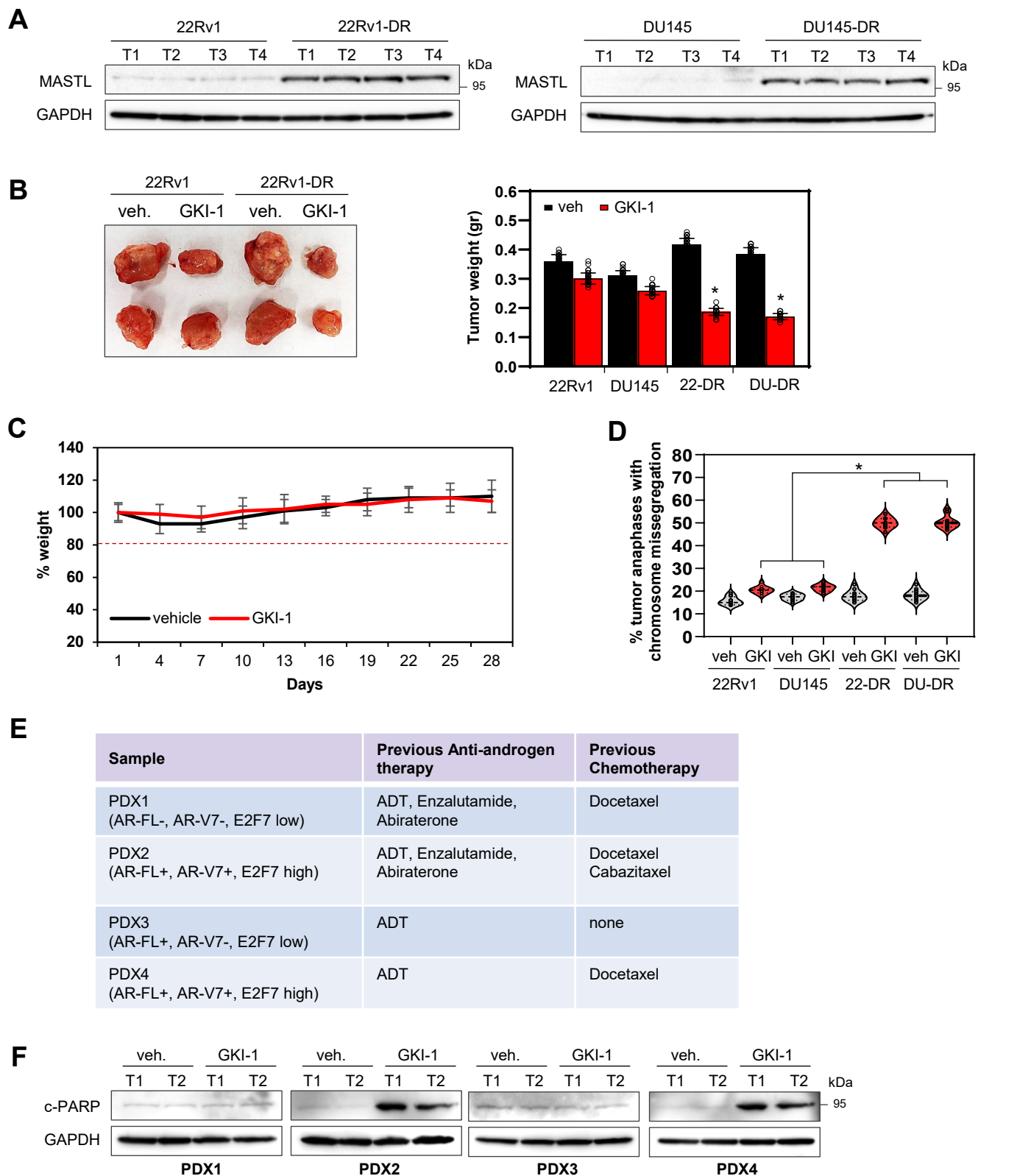
GAPDH

PDX1   PDX2   PDX3   PDX4

Figure S7. GKI-1 decreases growth of MASTL-addicted lethal PCa tumors. Related to Figure 7. (A) MASTL immunoblots in parental and syngenic DR xenograft tumors. **(B)** Representative images and tumor weights of parental/DR xenografts (n=40 per treatment condition) from mice treated with vehicle (DMSO) or GKI-1 for 28 days. 40 xenografts were analyzed for each treatment condition. **(C)** Weight loss of mice (n=10 per treatment condition) **B**). **(D)** Percentage of anaphases with lagging chromosome scored in parental and DR xenografts (n=12 per each treatment) from mice treated with vehicle (DMSO) or GKI-1for 4 days. **(E)** Table summarizing PDX sample name with details on AR, AR-V7 and E2F7 expression and previous anti-androgen and chemotherapy treatment received. **(F)** Cleaved PARP immunoblots in PDX models treated with vehicle (DMSO) or GKI-1 for 4 days. Unless indicated, GKI-1 administered at 100mg/kg/day i.p. *p $\leq$ 0.05, calculated using a two-tailed Student's t-test.